Characterization of chromosomal architecture in Arabidopsis by chromosome conformation capture

Grob, Stefan ; Schmid, Marc W ; Luedtke, Nathan W ; Wicker, Thomas ; Grossniklaus, Ueli

Abstract: BACKGROUND: The packaging of long chromatin fibres in the nucleus poses a major challenge, as it must fulfil both physical and functional requirements. Until recently, insight into the chromosomal architecture of plants was mainly provided by cytogenetic studies. Complementary to these analyses, chromosome conformation capture technologies promise to refine and improve our view on chromosomal architecture and to provide a more generalized description of nuclear organization. RESULTS: Employing circular chromosome conformation capture, this study describes chromosomal architecture in Arabidopsis nuclei from a genome-wide perspective. Surprisingly, the linear organisation of chromosomes is reflected in the genome-wide interactome. In addition, we study the interplay of the interactome and epigenetic marks and report that the heterochromatic knob on the short arm of chromosome 4 (hk4s) maintains a pericentromere-like interaction profile and interactome despite its euchromatic surrounding. CONCLUSION: Despite the extreme condensation that is necessary to pack the chromosomes into the nucleus, the Arabidopsis genome appears to be packed in a predictive manner, according to the following criteria: heterochromatin and euchromatin represent two distinct interactomes; interactions between chromosomes correlate with the linear position on the chromosome arm; and distal chromosome regions have a higher potential to interact with other chromosomes.

DOI: https://doi.org/10.1186/gb-2013-14-11-r129

Genome Biology

Characterization of chromosomal architecture in Arabidopsis by chromosome conformation capture

Genome Biology 2013, **14**:R129 doi:10.1186/gb-2013-14-11-r129

Stefan Grob (sgrob@botinst.uzh.ch)
Marc W Schmid (schmid.m@access.uzh.ch)
Nathan W Luedtke (luedtke@oci.uzh.ch)
Thomas Wicker (wicker@botinst.uzh.ch)
Ueli Grossniklaus (grossnik@botinst.uzh.ch)

ISSN 1465-6906

Article type Research

Submission date 18 June 2013

Acceptance date 5 November 2013

Publication date 24 November 2013

Article URL http://genomebiology.com/2013/14/11/R129

Characterization of chromosomal architecture in *Arabidopsis* by chromosome conformation capture

Stefan Grob[1]
Email: sgrob@botinst.uzh.ch

Marc W Schmid[1]
Email: schmid.m@access.uzh.ch

Nathan W Luedtke[2]
Email: luedtke@oci.uzh.ch

Thomas Wicker[1]
Email: wicker@botinst.uzh.ch

Ueli Grossniklaus[1*]
[*] Corresponding author
Email: grossnik@botinst.uzh.ch

[1] Institute of Plant Biology and Zürich-Basel Plant Science Center, University of Zürich, Zollikerstrasse 107, CH-8008 Zürich, Switzerland

[2] Institute of Organic Chemistry, University of Zürich, Winterthurerstrasse 190, CH-8057 Zürich, Switzerland

Abstract

Background

The packaging of long chromatin fibres in the nucleus poses a major challenge, as it must fulfil both physical and functional requirements. Until recently, insight into the chromosomal architecture of plants was mainly provided by cytogenetic studies. Complementary to these analyses, chromosome conformation capture technologies promise to refine and improve our view on chromosomal architecture and to provide a more generalized description of nuclear organization.

Results

Employing circular chromosome conformation capture, this study describes chromosomal architecture in *Arabidopsis* nuclei from a genome-wide perspective. Surprisingly, the linear organisation of chromosomes is reflected in the genome-wide interactome. In addition, we study the interplay of the interactome and epigenetic marks and report that the heterochromatic knob on the short arm of chromosome 4 (*hk4s*) maintains a pericentromere-like interaction profile and interactome despite its euchromatic surrounding.

Conclusion

Despite the extreme condensation that is necessary to pack the chromosomes into the nucleus, the *Arabidopsis* genome appears to be packed in a predictive manner, according to the following criteria: heterochromatin and euchromatin represent two distinct interactomes; interactions between chromosomes correlate with the linear position on the chromosome arm; and distal chromosome regions have a higher potential to interact with other chromosomes.

Background

In eukaryotic nuclei, chromosomes of considerable length are densely packed into a very small volume. In *Arabidopsis*, chromatin with a total length of about 8 cm has to be packaged into a nucleus of about 70 μm^3 and 5 μm diameter [1,2]. Nonetheless, the extremely dense packaging of chromatin does not lead to a chaotic entanglement of chromatin fibres. Eukaryotes have evolved mechanisms to untangle chromatin and to organise the nucleus into structural domains, facilitating chromosome packaging and, hence, the accessibility of the information stored within chromosomes. Therefore, chromosomal architecture is likely to influence the transcriptional states of a given cell and might be a major player in the epigenetic regulation of cell fate.

Over the last years, the field of epigenetics has grown rapidly, addressing basic questions about the long-term regulation of genes and how diverse cell types reach their differentiated states. These studies provided insights into the mechanisms that enable cells to differentiate into diverse cell types with distinct phenotypes despite sharing exactly the same genotype.

To date, most commonly studied epigenetic processes involve covalent modifications of DNA, such as cytosine methylation, and modifications of the core Histone proteins H3, H4, and their variants. Thereby chromatin can be grouped into activating and repressive chromatin states, defined by their epigenetic landscape. Among the main players are trimethylation of lysine 36 of H3 (H3K36me3) and dimethylation of lysine 4 of H3 (H3K4me2) that act as activating marks, and monomethylation of lysine 27 of H3 (H3K27me1) and dimethylation of lysine 9 of H3 (H3K9me2), which are associated with the repressive state [3-5].

Although studied for over a hundred years [6], *e.g.* with respect to cell division, chromosomal architecture - and thus higher-order chromatin organisation - has not been a major focus of epigenetic research. The lack of high-resolution techniques made structural studies of the nucleus extremely difficult. Nevertheless, chromatin condensation, and therefore chromosomal architecture, could be viewed as the first epigenetic mark described [7,8]. Recently, it became possible to study chromosomal architecture in more detail, on both a global and a local scale, for instance with respect to physical interactions between enhancers and promoters (*e.g.* [9,10]).

In plants, chromosomal architecture has been studied for many years using cytogenetic techniques and microscopic observations. Early studies allowed the discovery of basic chromosome conformations, heterochromatin and euchromatin, which was first described in mosses by Emil Heitz as early as 1929 [7]. Most condensed chromatin, or heterochromatin, is associated with centromeric regions. However, large heterochromatic regions outside the pericentromeres were also detected and, according to their microscopic appearance, were

termed knobs. Although first observed and best described in maize [11], knobs were also shown to exist in the model plant *Arabidopsis* on chromosomes 4 and 5 [12-14]. The heterochromatic knob on the short arm of chromosome 4 (*hk4s*) is derived from an inversion event, which brought a pericentromeric region to lie in a more centrally located region of the chromosome arm. Due to its length of 750 kb, *hk4s* is easily detectable, and is therefore the best studied knob in *Arabidopsis*. In contrast, the merely 60 kb long knob on chromosome 5 is only poorly described. Despite its central - and therefore euchromatic - position on the chromosome arm, *hk4s* kept the heterochromatic features of its pericentromeric origin. The knob *h4ks* is characterised by low gene density and an abundance of highly repetitive sequences, *e.g.* transposable elements.

To date, two methods are frequently used to study chromosomal architecture. Based on microscopic observations, fluorescence *in situ* hybridisation (FISH) visualises chromosomal architecture by detecting specific sections of chromosomes through hybridization with fluorescently labelled probes. Over the last decade, a completely different set of methods has been developed, which are summarised as chromosome conformation capture - in short 3C - technologies [15,16]. 3C uses formaldehyde cross-linked chromatin that is subsequently digested and religated. This produces circular DNA comprised of two restriction fragments that were initially in close spatial proximity within the nucleus. The abundance of these circular 3C templates can then be used to calculate interaction frequencies between two given fragments in the genome. In animal model systems and yeast, various studies have successfully employed 3C technologies since the first publication in 2002 [15]. Whereas 3C is employed to analyse pair-wise interactions (one specific fragment interacting with another specific fragment; *i.e.* one to one), circular chromosome conformation capture (4C) identifies interactions genome-wide to a viewpoint of interest [17] (*i.e.* one to all). HiC, the most recent 3C technology, facilitates the analysis of genome-wide interactions from all restriction fragments of a genome (*i.e.* all to all) [18].

In the plant field, however, the adoption of these technical advances was slower, such that only a few studies have been performed employing 3C technology. A study in maize revealed chromatin looping at the paramutagenic *b1* locus using 3C [19]. In *Arabidopsis*, to our knowledge, only two studies were published to date. Moissiard and colleagues compared global changes in the interactome between mutant *atmorc6* and wild-type plants [20]. However, this study did not focus on a detailed description of the chromosomal architecture of *Arabidopsis* nuclei. Another recent study showed the importance of local DNA looping for the correct expression of the flowering time regulator locus *FLC* [21].

Here, we provide insights into the general architecture of the *Arabidopsis* nucleus, using 4C applied to several viewpoints followed by Illumina sequencing. Our study aimed at characterizing global principles of chromosomal interactions as well as their correlations with epigenetic marks. Additionally, we found that the heterochromatic knob *hk4s* is characterised by a distinct interactome, which strongly resembles its pericentromeric origin.

Results

Our knowledge on chromosomal architecture in *Arabidopsis* is largely based on microscopic observations. Therefore, we aimed to gain insights into higher order chromatin organization based on 4C technology, which promises to complement previously published FISH experiments and to reveal novel mechanisms governing chromosomal architecture.

We performed 4C experiments on aerial tissue of two-week-old *Arabidopsis* seedlings using thirteen specific restriction fragments (viewpoints) distributed across all five chromosomes (Figure 1A). Employing high-throughput sequencing, 4C technology identifies sequences that physically interact with a given viewpoint. Therefore, the position and number of mapped 4C sequencing reads define the interactome of the given restriction fragment (i.e. the viewpoint) in space (position) and frequency or specificity (number of reads).

Figure 1 Primary 4C data analysis. (A) Schematic representation of the viewpoints chosen for this study. Viewpoints were named according to nearby genes or according to a region of special interest (*hk4s*). **(B)** Cluster analysis representing the reproducibility of biological duplicates. Letters A and B at the end of the names indicate biological replicates. **(C)** Power law scaling, indicative for the interaction decay for all viewpoints across a distance to the viewpoint from 1 kb to 10 Mb.

To cover a wide distribution of chromosomal interactions, we chose viewpoints that reside in various locations: from pericentromeric, to mid-chromosome arm, to distal positions (Figure 1A).

Data evaluation reveals robustness of 4C experiments

To obtain the interactome of a given viewpoint, short sequence reads were mapped to restriction fragments and subsequently merged into sliding windows consisting of 100 *Hind*III restriction fragments. We then assigned *P*-values to each window describing the specificity of the interaction to a given viewpoint. To obtain these *P*-values, read counts of 4C windows were compared to probabilities of a normal distribution. The parameters of this distribution were calculated using 1000 sets of windows, each generated by random shuffling of 4C fragments. As chromosome arms differ considerably in their length and, therefore, their DNA amount, we calculated *P*-values individually for each chromosome arm. Windows with *P*-values ≤ 0.01 where defined as specifically interacting with their corresponding viewpoint and are, hereafter, referred to as preys.

The mappability of sequencing reads poses a major concern for any genomic study. Due to the incomplete assembly of centromeric repeats in the *Arabidopsis* reference genome, we excluded regions within 100 kb distance of the centromere. Visual inspection of genomic Illumina sequencing data revealed an even distribution of mapped reads along the remaining chromosome sequence and, therefore, no other major mappability biases were identified.

To assure the reproducibility of this study, 4C experiments were performed in duplicates. Correlations between duplicates and different viewpoints were calculated using the sum of reads per window. Spearman correlation coefficients were high for duplicates (mean = 0.88, sd = 0.07), and relatively low for different viewpoints (mean = 0.26, sd = 0.31). However, interacting viewpoints and viewpoints located in close proximity (see Figure 1A), such as the two viewpoints at the *MEDEA* (*MEA*) locus, show correlation coefficients close to those of replicates of the same viewpoint. Cluster analysis supports these findings (Figure 1B), further demonstrating that viewpoints on the same chromosome arm also show higher correlations among each other than with viewpoints located on other chromosomes arms.

Taken together, these analyses reveal the robustness of our data.

To differentiate between random interactions, which are mainly dependent on chromosomal proximity to the viewpoint, and specific interactions, we estimated the genomic distance-dependent decay of the interaction probability on a distance of 1 kb – 10 Mb from the viewpoint. For this, we pooled 4C reads of all viewpoints within the given distance to their viewpoints. Performing linear regression on logarithmized distance and contact probabilities, we calculated a slope of −0.73, i.e. the contact probability decays with a power law function of distance$^{-0.73}$ (Figure 1C). This result resembles similar analyses of the *Drosophila* (−0.85) [22] and human (−1.08) [18] genomes.

Cis-interactions are enriched within chromosome arms

Since the replicate correlation was high, we pooled replicates for a common representation of the 4C interactome (Figure 2A, Figure 2B) using the software Circos [23]. Figure 2C illustrates an example of a more detailed representation of 4C interactomes for the *FIS2* viewpoint. All other representations of individual viewpoints are shown in Additional files 1: Figure S1, 2: Figure S2, 3: Figure S3, 4: Figure S4, 5: Figure S5, 6: Figure S6, 7: Figure S7, 8: Figure S8, 9: Figure S9, 10: Figure S10, 11: Figure S11, 12: Figure S12, 13: Figure S13. At first sight, we observed an apparent enrichment in inter-chromosomal interactions of distal regions of chromosomes (Figure 2A). Additionally, intra-chromosomal interactions appear to be mostly occurring locally around the viewpoint and between distal regions of the two chromosome arms (Figure 2B and Figure 2C).

Figure 2 Summary of 4C interactomes. Circos plots illustrate the 4C interactome, transcription rate, and chromosomes with euchromatic and centromeric regions. Line colour refers to the colour of the viewpoint names at the periphery of the Circos plots. Only interactions with a *P*-value < 10^{-3} are plotted. **(A)** *Trans*-interactions **(B)** *Cis*-interactions. **(C)** 4C interactome of viewpoint *FIS2*. Colour code refers to significance levels. Gene density (blue circles) and transposable element density (purple circles) are indicated to illustrate to occurrence of heterochromatin and euchromatin. The region covered by the knob *hk4s* is highlighted with a transparent rectangle on the short arm of chromosome 4. Interaction values equal to $\sum_i(\log_2(\text{number of reads in fragment}_i))$, where i stands for a fragment within a given window, are scaled to the viewpoint's total library size.

Interactions can be categorised into *cis*- and *trans*-interactions, which require different analysis techniques [24]. *Cis*-interactions (Figure 2B) refer to within chromosome interactions, whereas *trans*-interactions (Figure 2A) are defined as in-between chromosome interactions.

By visual inspection of the interaction frequencies, we observed that local interactions rarely spread across the centromeres, (Figure 2B, Figure 2C, Additional files 1: Figure S1, 2: Figure S2, 3: Figure S3, 4: Figure S4, 5: Figure S5, 6: Figure S6, 7: Figure S7, 8: Figure S8, 9: Figure S9, 10: Figure S10, 11: Figure S11, 12: Figure S12, 13: Figure S13), indicating that interactions between the two arms of the same chromosome (*i.e. inter*-arm interactions) are distinct from *intra*-arm interactions, thus splitting *cis*-interactions into two groups.

Therefore, we asked whether chromosomes or rather chromosome arms are the basic unit of nuclear architecture. To answer this question, we calculated the average number of reads per million (RPM) for each chromosome arm and defined three chromosome arm types: The chromosome arm hosting the viewpoint (viewpoint-arm), the other arm on the same chromosome as the viewpoint (*cis*-arm), and arms of all other chromosomes (*trans*-arms). We

observed the highest interaction frequencies and, therefore, the highest mean RPM values within the viewpoint-arm (Figure 3A), showing that a high proportion of chromosomal interactions occur within the same arm.

Figure 3 Physical constraints of chromosomal architecture. (A) Number of reads per million of four distinct classes of interactomes. Viewpoint: 4C reads that map on the same chromosome arm as the viewpoint. Viewpoint (removed): Interactions mapping the viewpoint's arm, excluding interactions, that map within 2 Mb distance to the viewpoint. *Cis*: 4C reads that map to the other arm of the chromosome harbouring the viewpoint's arm. *Trans*: 4C reads that map to all other chromosome arms. Red represents replicate A, blue represents replicate B. **(B)** Relative distance to the centromere (0 at the centromere, 1 at the telomere) in which 50% of the 4C reads can be found depends on the relative distance of the viewpoint to the centromere. Red circles represent Replicate A, blue circles represent Replicate B. **(C)** The percentage of 4C reads that can be mapped to *trans*-arms is positively correlated with the viewpoint's absolute distance to the centromere in base-pairs (bp). Red circles represent Replicate A, blue circles represent Replicate B.

Interactions with the *cis*-arm are significantly more frequent than with *trans*-arms (Student's t-test, p = 0.0135 for replicate A and p = 0.0129 for replicate B). However, the differences are small compared to the viewpoint-arm RPM values and the *cis*-arm RPM values (Student's t-test, $p = 1.4*10^{-13}$ for replicate A and $p = 1.7*10^{-13}$ for replicate B) (Figure 3A). A large proportion of interactions within the viewpoints-arm occur within close vicinity of the viewpoint itself. To investigate whether also long-range interactions preferentially occur within the viewpoint's arm, we excluded regions surrounding the viewpoints by 2 Mb on each side of the viewpoint (Figure 2A). Devoid of the viewpoint's region, the RPM values are strongly reduced; however, they are still significantly higher than RPM values of *cis*-arms (Student's t-test, *P*-value = 0.012 for replicate A and *P*-value = 0.01 for replicate B).

The difference between *trans*-arms and *cis*-arm appears to be dependent on the distance of the viewpoint from the centromere. Distal viewpoints (*e.g. MEA* and *CYTOKININ-INDEPENDENT1* (*CKI1*), see Additional files 1: Figure S1, 2: Figure S2 and 6: Figure S6) did not appear to preferentially interact with their respective *cis*-arm compared to the *trans*-arm. This can been observed by comparing overall interaction values of the viewpoint's respective *cis*-arm compared to the overall interaction values of *trans*-arms. In contrast, viewpoints residing in the vicinity of the centromeres (*e.g. YAOZHE* (*YAO*), *AT3G44380*, see Additional files 7: Figure S7 and 10: Figure S10) exhibit increased *cis*-arm interactions compared to *trans*-arm interactions and, thus, limited spreading of local interactions across the centromere.

In summary, *intra*-arm interactions are about 10-fold more frequent than *inter*-arm interactions, whereas *inter*-arm and *inter*-chromosomal interactions differ by about 2-fold on average. Therefore, our results show that chromosome arms are the main interaction unit and that interaction frequencies decrease sharply close to the centromeres.

Linear position along the chromosome influences the viewpoint's interaction potential

We found that *trans*-interactions can make up to 50% of the total interactome of a given viewpoint. Therefore, we were interested in understanding the mechanisms governing *trans*-interactions. Visual inspection of 4C data (Figure 2A, Figure 2C, Additional files 1: Figure

S1, 2: Figure S2, 3: Figure S3, 4: Figure S4, 5: Figure S5, 6: Figure S6, 7: Figure S7, 8: Figure S8, 9: Figure S9, 10: Figure S10, 11: Figure S11, 12: Figure S12, 13: Figure S13) suggested an effect of the viewpoints' positions along the chromosome arms on the *trans*-interaction frequencies. We hypothesised that chromosomal interactions are not solely reflecting specific functions of a given region but are rather a consequence of physical constraints. To investigate whether the viewpoint's positioning along the chromosome arm is a major constraint for *trans*-interactions, we tested whether regions with similar distance to the centromeres are more likely to interact.

We calculated the relative distance to the centromeres where 50% ($dist_{0.5}$) of all 4C reads could be found. As a considerable proportion of all interactions can be found surrounding the viewpoint and would therefore distort the analysis, we excluded the viewpoint's arm. A significant correlation between $dist_{0.5}$ and the relative distance of the viewpoint to the centromere could be observed (Spearman correlation coefficient = 0.722, *P*-value of linear model = $3.4*10^{-28}$) (Figure 3B). This suggests that regions with a similar relative distance to their corresponding centromeres are likely to co-localise with each other in the 3-dimensional space of the nucleus. The observation is most pronounced in distal regions; however, it is also observable in regions in proximity to the pericentromeres.

Distal chromosomal regions show an increased *trans*-interaction potential

We hypothesised that the flexibility of a chromosome arm is a major physical constraint, influencing the interaction potential of a viewpoint. Assuming that centromeres act as chromosomal anchors, distal regions of chromosome arms should exhibit a higher flexibility than regions close to the centromere (e.g. [25-28]). Hence, we predicted that distal viewpoints should exhibit an increased *trans*-interaction potential.

Therefore, we tested the correlation between the absolute distance of the viewpoint to the centromere and the reads per kilobase per million (RPKM) of 4C reads found in *trans* (including the *cis*-arm) (Figure 3C). Distal viewpoints were shown to interact more frequently with regions in *trans* than viewpoints that reside closer to the centromere (Spearman Correlation Coefficient = 0.774, *P*-value of linear model = 10^{-5}) (Figure 3C).

These results indicate that the localisation of a viewpoint along the chromosome arm significantly influences its interaction pattern.

Principal component analysis shows correlation between the epigenetic landscape and the interactome

The interplay of epigenetic marks, such as histone modifications, and physical interactions of two sequences were previously shown to be important for stringent gene regulation [21,22,29,30]. Therefore, we investigated whether specific epigenetic marks can be correlated with long-range interactions.

We obtained previously published histone modification data [31], specifically H3K4me2, H3K4me3, H3K9me2, H3K27me1, H3K27me3, H3K36me2, H3K36me3, H3K9Ac, and H3K18Ac. From the same data set, we included transcriptome, histone H3 occupancy, and genomic DNA control data. Additionally, we obtained publically available CG, CHH, and CHG methylation data [32]. Since data obtained from Chromatin Immunoprecipitation (ChIP) for histone modifications cannot be directly compared to 4C data due to the different

scaling of the two data sets [24], we calculated density values of each epigenetic feature, within 4C windows. We analysed the epigenetic modification densities (EMDs) as the sum of nucleotides covered with at least one uniquely alignable short sequence, divided by the total number of nucleotides for each individual 4C restriction fragment (i.e. the length of the restriction fragment). Subsequently, the mean for each window was calculated. To adjust the scale of the 4C data to the EMDs, we chose a window size of 25 fragments, which still confers satisfactory reproducibility between replicates. 4C windows were categorised in prey regions (windows, which show an interaction probability of ≤ 0.01) and randomly chosen control regions.

If specific histone modifications or sets of histone modifications are associated with an interaction pair, one could assume that prey regions of a given viewpoint share a common epigenetic environment, reflected by a particular composition of the EMDs. To elucidate how histone modifications are related to the interactome, we performed principal component analysis (PCA) (Figure 4A). For each viewpoint, the mean EMDs (selecting only histone modification data) of prey and control regions were calculated and included in the PCA. As the first principal component was shown to explain 97% of the total variation, it was the only component used for further analyses.

Figure 4 Crosstalk of epigenome and interactome. (A) Principal component analysis (PCA) using mean EMDs of control and prey regions for each viewpoint. EMDs included in the PCA were: H3K4me2, H3K4me3, H3K9me2, H3K27me1, H3K27me3, H3K36me2, H3K36me3, H3K9Ac, and H3K18Ac. Coloured arrows represent the two highest contributing EMDs to the variance of the first component in positive and negative direction, respectively. Note that the first principal component explains almost all the variance (97%). Therefore, only first principal component is plotted. Prey regions are represented by green dots, control regions by yellow dots. **(B)** Mean CG methylation densities of prey and control regions for individual viewpoints. The mean was calculated across 1000 times randomly sampled 50 prey and 50 control regions, respectively. Green bars represent preys and yellow bars represent controls. **(C)** Examples of the interactome-epigenome interplay for three different viewpoints and one of their corresponding prey regions. Top track: log summed 4C reads per window (100 fragments, starting every fragment). 4C reads of replicate A are plotted in the positive intercept, 4C reads of replicate B are plotted in the negative intercept. Middle Track: EMD of the highest contributing factors of the PCA in positive and negative direction, respectively. In order to achieve comparable representation of H3K36me3 and H3K27me1 densities, the density of every window (25 fragments, starting every 5 fragments) was divided by the mean density of each histone modification. Arrowheads point at regions where the 4C interactome and local EMD peaks appear to correlate. *FWA*: viewpoint on chromosome 4, 12–14 Mb; prey on chromosome 5, 23 Mb - 25 Mb. *PHE*: viewpoint on chromosome 1, 23.5 - 25.5 Mb; prey on chromosome 1, 20–22 Mb. *hk4s*: viewpoint on chromosome 4, 0.8 - 2.8 Mb; prey on chromosome 2, 4–6 Mb.

Two opposing groups of EMDs, H3K36me3/H3K4me2 and H3K27me1/H3K9me2, are the major contributors to the first principal component of the PCA, and are indicated as arrows in Figure 4A. Closer observation of three viewpoint/prey pairs reveals how EMDs and interaction frequencies are coupled (Figure 4C). Euchromatic viewpoints, such as *FLOWERING WAGENINGEN* (*FWA*) (Figure 4C – top row), which are characterised by low levels of H3K27me1 and enrichment of H3K36me3, preferentially interact with regions with a similar EMD pattern. This is evident from increased H3K36me3 levels surrounding the region of high interaction frequencies and local peaks of H3K27me1 enrichment, coinciding

with a significant drop in interaction frequencies (Figure 4C, top row, right panel). In contrast, heterochromatic viewpoints (Figure 4C - middle and bottom row), which are characterised by the inverse EMD composition, preferentially interact with regions exhibiting low H3K36me3 and high H3K27me1 levels. For example, local enrichment of H3K27me1 coincides with increased interaction frequencies to *PHE1* (Figure 4C, middle row, right panel). Additionally, the asymmetric local interactions surrounding *hk4s* appears reflected by the asymmetric distribution of H3K27me1 (Figure 4C, bottom row, left panel).

Additionally, we performed PCA separately for individual viewpoints, as illustrated in Additional file 14: Figure S15. Although the same EMDs can be identified as major factors for most viewpoints, the first component of the PCA is less dominant, indicating a more complex collaboration of factors separating control regions from prey regions. Furthermore, various viewpoints do not show a very clear separation of prey and control regions. Interestingly, this is most evident for viewpoints whose preys are associated with heterochromatic marks (*PHERES1* (*PHE1*), *hk4s*, *AT1G51860*, Additional file 14: Figure S15).

To address the individual contribution of epigenetic marks to the interactome, we performed a test based on a modified Gene Set Enrichment Analysis (GSEA) [33]. In summary, we tested whether prey regions show a non-random distribution in their EMD profiles (see Materials and Methods for a detailed description). The obtained empirical *P*-values are indicative for the likelihood of a random set of regions to show a similar EMD value distribution as the tested prey regions (Table 1).

Table 1 Analysis of the epigenetic landscape

Genomic Feature	Permutation Test	GSEA-like Test
	P-value	P-value
H3	0.1013	0.0779
H3K18Ac	**0.0335**	**0.0178**
H3K27me1	**0.0249**	**0.0084**
H3K27me3	0.3355	0.099
H3K36me2	**0.0033**	**0.0051**
H3K36me3	**0.0033**	**0.0054**
H3K4me2	**0.0033**	**0.0051**
H3K4me3	**0.0037**	**0.0051**
H3K9Ac	**0.0033**	**0.0051**
H3K9me2	**0.0325**	**0.0057**
Transcription	**0.0033**	**0.0054**
CG methylation replicate 1	**0.0065**	**0.0054**
CHG methylation replicate 1	**0.0083**	**0.0051**
CHH methylation replicate 1	**0.0083**	**0.0051**
CG methylation replicate 2	**0.0083**	**0.0054**
CHG methylation replicate 2	**0.0087**	**0.0051**
CHH methylation replcate 2	**0.0083**	**0.0051**
genomic DNA	0.0871	0.056

Table contains adjusted *p*-values (FDR) for genomic features tested with a permutation test or a GSEA-like algorithm. Genomic features differing significantly between prey and control regions are highlighted in bold (alpha = 0.05).

To independently investigate whether control and prey regions significantly differ for individual epigenetic features, we developed a permutation test. In a first step, we calculated for each viewpoint the mean density for each epigenetic feature (Figure 4B and Additional file 15: Figure S16). Epigenetic features that coincide with the occurrence of heterochromatin and euchromatin, such as DNA methylation, clearly split the viewpoints into two groups: Whereas viewpoints such as *PHE1*, *AT1G51860*, and *hk4s* have high methylation levels in their prey regions and low methylation levels in control regions, viewpoints that occur in euchromatin show an inverse pattern. Similar patterning is also detectable for other epigenetic modifications (Figure 4B and Additional file 15: Figure S16). The inverse patterning of the epigenetic landscape between different viewpoints makes it difficult to perform statistical tests using EMD values directly.

Therefore, we calculated the absolute difference in the epigenetic feature's density between control and prey regions. In essence, we tested whether the absolute difference in EMD values between prey and control regions are significantly different from the absolute difference between two sets of randomly selected regions. As a test set, we shuffled the 50 prey and 50 control regions into two randomized groups. As for prey and control regions, we then calculated means and subsequently absolute differences between the two randomized groups. By repeating the permutations 1000 times, we obtained a distribution of absolute differences between the two randomized groups for each epigenetic feature. This allowed us to calculate empirical *P*-values, which describe the chance that two randomly selected regions differ more in their EMD setup than prey and control regions (Table 1).

In line with the previously performed PCA, both tests revealed that the densities of most epigenetic features significantly differ between control and prey regions (Table 1). Histone H3 occupancy, however, did not significantly differ between the two groups, indicating that histone density itself does not correlate with a viewpoint's interactome. Additionally, no significant difference in genomic control data could be observed, rendering possible sequencing and alignment biases of the analyzed EMD data set unlikely.

In summary, we conclude that the epigenetic landscape coincides with the interactome. This is mainly reflected by distinct euchromatic and heterochromatic interactomes.

The heterochromatic knob evades its euchromatic environment

Analyzing the read numbers of a first set of 4C viewpoints, we consistently observed a drop in read numbers for a region situated in the centre of the short arm of chromosome 4 (Figure 5B and Additional files 1: Figure S1, 2: Figure S2, 3: Figure S3, 4: Figure S4, 5: Figure S5, 6: Figure S6, 7: Figure S7, 8: Figure S8, 9: Figure S9, 10: Figure S10, 11: Figure S11, 12: Figure S12, 13: Figure S13). Surprisingly, this drop in interaction frequency was observed irrespective of the location of the viewpoint. Additionally, we did not observe this drop by visual inspection of genomic sequencing data, implying no mappability bias. Therefore, we hypothesised that global constraints of chromosomal architecture govern genome-wide interactions with this region.

Figure 5 Interactome of the knob *hk4s*. **(A)** Circos plot illustrating all *cis*- and *trans*-interactions of viewpoints located on chromosome 4. Only interactions with $P \leq 10^{-4}$ were considered. Line colour corresponds to the colour of the viewpoints name indicated at the periphery of the plot. Chromosomes are not drawn to scale. **(B)** Representation of interaction frequencies for viewpoints situated on chromosome 4**.** Note that only the region up to 4 Mb is plotted. Therefore, viewpoints *AG* and *FWA* cannot be seen. Black dots: positions of viewpoints; turquois dots: genes; violet dots: transposable elements; light grey: euchromatic chromosomal segment; dark grey: heterochromatic chromosomal segments; dark grey ellipse: centromere. **(C)** Model of a potential mid-range chromosomal loop, connecting *hk4s* with the centromere of chromosome 4.

Exploring the region in more detail, we found that it corresponds to the heterochromatic knob (*hk4s*), which is cytogenetically detectable and has been described earlier [12,34] (Additional file 9: Figure S9).

To analyse the implications of *hk4s* on chromosomal architecture in more detail, we designed three additional 4C assays. We set a viewpoint within *hk4s* and two viewpoints flanking *hk4s* in a more distal (*SWINGER* (*SWN*)) and proximal region (*YAO*) of the short arm of chromosome 4. As the flanking viewpoints were set relatively close to *hk4s*, we expected increased frequencies of interactions within the knob and the viewpoints due to the previously observed local enrichment of interactions surrounding the viewpoints. However, the local interaction frequency of both neighbouring viewpoints dropped sharply on the borders of *hk4s* (Figure 5A, Figure 5B, Additional files 8: Figure S8, 9: Figure S9, 10: Figure S10). *YAO* (coordinate at 2.75Mb) is situated adjacent to the border of the pericentromere (coordinates 2.78Mb- 5.15Mb) [3]. Interestingly, the local interaction pattern appears to be asymmetric. We observed a loss of specific interactions not only along the boundary to the knob but also along the much closer border of the pericentromeric region (Figure 5B, Additional file 10: Figure S10). The defined sharp boundaries for local *YAO* interactions resemble the interaction pattern of *hk4s*. Whereas *YAO* resides in euchromatin surrounded by heterochromatin, *hk4s* can be viewed as its counterpart, residing in heterochromatin but surrounded by euchromatin (Figure 5B).

Regions situated on the long arm of chromosome 4 (*AGAMOUS* (*AG*) and *FWA*) strongly interact with regions surrounding *hk4s,* including *YAO*, but not with *hk4s* itself (Figure 5B, Additional files 11: Figure S11 and 12: Figure S12), resembling the sharp drop in interaction frequencies of *SWN* and *YAO* (Figure 5A, Figure 5B, Additional files 8: Figure S8, 9: Figure S9, 10: Figure S10).

Consistent with observations for the two flanking viewpoints, the significant local interaction frequencies of the viewpoint set in the centre of *hk4s* were limited by the borders of the knob. Additionally, we observed strong interactions of *hk4s* with pericentromeric regions of chromosome 4 and the pericentromeres of other chromosomes (Figure 5A). The apparent absence of specific interactions between *hk4s* and the pericentromere of the short arm of chromosome 4 is likely due to an artefact of the method to assign *P*-values. Indeed, as *P*-values were calculated for individual chromosome arms, the high number of reads covering the viewpoint itself masks other regions on the same chromosome from being associated with low *P*-values.

Discussion

Replication and the choice of appropriate window size are key to ensure robustness of 4C

Based on correlation analysis of biological replicates, we show that 4C interaction profiles in *Arabidopsis* can be reproducibly obtained. However, reproducibility is dependent on the window size chosen. As chromosomal interactions are dynamic and partly stochastic, one single restriction fragments of two replicates can vary considerably in read number. Taking windows consisting of several fragments into account, can balance this variation. As we were mainly interested in the global architecture of the *Arabidopsis* nucleus, we chose window sizes of up to 100 restriction fragments. However, the resolution to study short-range interactions is decreased by increasing the window size. Whereas 4C is well suited to study mid- and long-range interactions, it is not necessarily the method of choice to study short-range interactions in *Arabidopsis* (*e.g.* promoter/enhancer interactions). Regulatory sequences that are presumably involved in short-range interactions, such as chromatin loops, are often separated by less than a few kb. They are, therefore, difficult to analyse using 3C technologies, which rely on a sufficient number of restriction sites between the two regions of interest to confer satisfactory resolution.

Arabidopsis and *Drosophila* show comparable chromatin compaction and genome size

The interaction decay exponent describes the slope with which the interaction probability decays from the viewpoint. Therefore, it can provide an approximation for regional chromosomal compaction. Theoretically, a steeper slope indicates decreased flexibility of a given viewpoint, as distant regions are less likely to interact with it. Decreased flexibility can be interpreted as higher local chromatin compaction. *Drosophila* and *Arabidopsis* are similar with respect to chromosome number, genome size, total number of genes, and nuclear volume [1,35]. These characteristics could lead to similar constraints of chromosomal architecture. The interaction decay exponent determined in this study (−0.73) is close to the one described earlier for *Drosophila* (−0.85) [22]. Interestingly, the interaction decay exponent in human nuclei is lower (−1.08), implying higher local compaction [18]. This observation is consistent with physical characteristics of human nuclei compared to those in *Arabidopsis* and *Drosophila*. Although varying considerably, human nuclei show a lower volume/DNA ratio than nuclei in *Drosophila* and *Arabidopsis*, indicating a higher global chromatin compaction [35]. It is important to mention, however, that interaction decay exponents cannot be compared very easily between different studies, as the calculated exponents of the power law scaling depend on the range of distances used for calculations. However, which scale best describes an overall distance dependent interaction decay is a matter of debate. Additionally, the slope with which interactions decays, was previously shown to vary between domains of different epigenetic landscape [18,22]. We observe a variation of interaction decay exponents among the different viewpoints from −0.56 to −0.96 (Additional file 16: Figure S14). However, we could neither explain these differences by the positional nor by the epigenetic environment of a given viewpoint. Therefore, the global distance dependent interaction decay does not necessarily add to the understanding of how interaction frequencies decrease with distance from an individual viewpoint.

How and whether global nuclear compaction and interaction probability decay really correlate is not entirely clear. An exploration of the *Arabidopsis linc1, linc2* double mutant could possibly answer this question, as these plants were reported to exhibit an increased DNA density compared to wild-type plants [1].

4C results refine the view on general chromosomal architecture in *Arabidopsis*

The investigation of general features of chromosomal architecture in this study is consistent with previous findings studying *Arabidopsis* nuclei using cytogenetic methods [27,36]. However, 4C technology enables us to generate genome-wide interaction maps for various viewpoints and, hence, does not depend on a pair-wise analysis of two interacting sequences. This greatly adds to our understanding of general constraints on chromosomal architecture.

Basic interaction units appear to be defined as chromosome arms with centromeres acting as a boundary. These findings are in agreement with an earlier study by Schubert and colleagues reporting that chromosome arms are localised in distinct territories, as evidenced by FISH on *Arabidopsis* nuclei [36]. However, whether centromeres always act as strict boundaries cannot be conclusively answered as the boundary effect of centromeres is likely to vary between different the chromosomes.

We observed a strong influence of a viewpoint's chromosomal location on its interaction potential. Remarkably, the linear organisation of chromosomes is reflected in the overall interaction potential of a given viewpoint, despite the dense packaging of the genome in the nucleus.

We propose that centromeres anchor the chromosomes in the nucleus, thereby allowing chromosome arms to protrude inside the nuclear volume [25-28]. The flexibility of chromosome arms thus increases with their length, allowing distant regions to interact more frequently in *trans* than more centrally located regions. Our hypothesis is supported by strong evidence for centromere clustering and their adherence to the nuclear matrix in different model organisms [37-39]. Taken together, these findings may explain why regions with a similar distance to the centromeres, which act as anchor points, preferentially interact with each other.

We also observed significant inter-telomeric interactions. A high interaction frequency of (sub-)telomeric regions in *Arabidopsis* was recently also shown by FISH [36]. In addition, previously published HiC data suggest increased interaction frequencies between telomeres [20,38]. In contrast, telomeres and centromeres do not interact, indicating a strict separation of these two key organisational elements of *Arabidopsis* chromosomes. These findings are in line with previous studies and may be explained by the nucleolar localisation of telomeres [27,40].

Remarkably, in *Drosophila* long-range interactions seem to nearly exclusively occur within the viewpoint's chromosome arm [30]. In the present study, however, up to 50% of all interactions were found outside the viewpoint's chromosome arm. Whether this difference to *Drosophila* holds biological meaning is unclear. The presence of a higher number of individual cell types in the sample could theoretically increase the number of observable interactions and result in a more complex interactome of a given viewpoint. Such increased complexity could thereby lead to an increased number of *trans* interactions. However, we do not estimate the number of cell types to be significantly different in the present study and in

the report by Tolhuis and colleagues, in which 4C was performed on *Drosophila* larval brain tissue [30], as the aerial seedling tissue used in our study is predominantly composed of mesophyll cells. The phase of the cell cycle might be a more important confounding factor. Over a cell cycle, chromosomal architecture changes dramatically. Cells of *Arabidopsis* seedlings divide at high frequency, leading to a rather short period of time in which cells reside in interphase. Therefore, the proportion of cells in specific stages of the cell cycle could be a major factor influencing the (averaged) chromosomal conformation of a population of cells.

A viewpoint's interactome is reflected by its epigenetic landscape

PCA revealed two distinct groups of prey regions, discriminable mainly by the level of H3K36me3/H3K4me2 and H3K27me1/H3K9me2 densities. Interestingly, these histone modifications are commonly attributed to euchromatin or heterochromatin, respectively [31]. Furthermore, the heterochromatic pair H3K27me1/H3K9me2 is described to be the major component of "chromatin state 3", which is mainly associated with transposable elements, as previously reported by Roudier and colleagues, whereas the pair H3K36me3/H3K4me2 primarily contributes to "chromatin state 1", associated with active genes [3]. In *Drosophila*, Filion and colleagues describe five distinct chromatin types, distinguished by the composition of proteins adhering to the DNA. H3K4me2 was shown to be most abundant in "red chromatin", which represents one of two euchromatic chromatin states. In contrast, H3K9me2 is enriched in "green chromatin", which can best be described as the classical heterochromatin of pericentromeric regions [4]. As anticipated by previous cytological studies of *Arabidopsis* nuclei, the interactome obtained by 3C technologies can be separated into two distinct domains, correlating with both the epigenetic and the cytogenetic definition of heterochromatin and euchromatin. Interestingly, this distinction is not only confined to *cis*-interactions but can also be observed at the level of the whole genome. In addition, we suggest a further discrimination of heterochromatic interactions. The purely heterochromatic viewpoint *hk4s* predominantly interacts with visible heterochromatin such as the pericentromeric regions. *PHE1*, which shows moderate H3K27me1 enrichment surrounding the viewpoint, interacts predominantly with heterochromatic islands within otherwise euchromatic regions (see Figure 2, Figure 4C, and Additional file 4: Figure S4).

Previous work in *Arabidopsis* has shown that homologous pairing is decreased in hypomethylation mutants [41], indicating a role of cytosine methylation in long-range interactions. We observed significant differences between control and prey regions with respect to their CG, CHH, and CHG methylation densities. Additionally, transcription rates exhibit significant differences between prey and control regions. Whether transcriptionally active genes interact with each other is not clear, since the genes residing in our viewpoints are not evenly balanced regarding their transcriptional state (active *vs* silenced). This renders the viewpoints used in this study inappropriate for statistical analysis.

Taken together, we conclude that interactomes share a common epigenetic landscape, leading to distinguishable heterochromatic and euchromatic interactomes. However, it is not clear to what extend individual epigenetic modifications influence the interactome and to what extend the epigenetic landscape is cause or consequence of a given interactome.

The knob *hk4s* - exception or rule

Finally, the knob *hk4s* appears as an exceptional feature within the *Arabidopsis* nuclear landscape, as it predominantly interacts with pericentromeric regions. We think that *hk4s* represents the exception that proves the rule because its interactome reflects the pericentromeric origin of *hk4s*, which arose by an inversion that placed a pericentromeric region into the centre of the chromosome arm. As previously discussed, heterochromatic regions form a distinct interactome, in which heterochromatic islands that reside in an euchromatic environment are included. Figure 5C illustrates a model suggesting overall chromosomal architecture and chromosomal looping of *hk4s* to the clustered centromeres. Our results indicate that the knob *hk4s* acts as an interaction insulator for its neighbouring regions and conserved its pericentromeric origin with respect to its interaction frequencies.

To date, neither a functional role as a (neo)centromere nor an association with the nuclear matrix has been reported for *hk4s*. However, the specific interaction of *hk4s* with centromeres could raise speculations concerning the functional role of *hk4s* in the nucleus. The specificity of a given region to function as a centromere is surprisingly flexible. In maize, previous reports show that centromere identity is not irreversibly defined. Wolfgruber and colleagues demonstrated that the centromere of maize chromosome 5 has moved to a new location, due to the invasion of non-centromeric retrotransposons, splitting the centromere into two. Consequently, one of the two cleavage products lost its association with Histone CenH3, which defines centromeres epigenetically by replacing the regular Histone H3 protein [42]. In maize, centromere identity correlates with the abundance of centromeric retrotransposons [43], which specifically invade centromeric regions. Nevertheless, centromere identity appears to be mainly controlled epigenetically and not by DNA sequence [44,45]. However, previous reports show that that Histone CenH3 accumulation defines the functional centromere in *Arabidopsis* and that CenH3 is predominantly associated with the 178 bp centromeric repeats [46,47]. As the knob *hk4s* lacks the centromeric 178 bp repeats and is thought to originate from a pericentromic region, which is not associated with CenH3, we conclude that *hk4s* is mainly involved in heterochromatin formation and that *hk4s* is unlikely to play a role as a (neo)centromere.

Conclusions

Centromeres are key elements for chromosomal organisation as the position relative to the centromere strongly influences the interactome of a chromosomal region. We propose that the length of chromosome arms limits the mobility with which a region can traverse through the nuclear space and, therefore, influences the interaction potential in *trans*. Another hallmark of chromosomal architecture in *Arabidopsis* nuclei is the separation of two seemingly distinct interactomes, strongly correlating with visible heterochromatin and euchromatin. Interestingly, heterochromatic islands are partly able to evade their euchromatic context. The epigenetic landscapes of the heterochromatic and euchromatic interactome are clearly distinguishable. Therefore, histone modifications, which were previously described to be characteristic of chromatin states, may also be predictive for the interaction potential of a given chromosomal region.

Materials and methods

Nuclei extraction and 4C sample preparation

Seedlings of *Arabidopis thaliana* (L.) Heynh, accession Columbia (Col-0), were grown for 14days on MS plates. Aerial tissue of seedlings was collected (ca 10g per sample) and distributed evenly to 4 conical 50ml tubes. Under vacuum, the seedlings were incubated for 1h at room temperature (RT) in 15ml freshly prepared nuclei isolation buffer (NIB) (20mM Hepes (pH8), 250mM sucrose, 1mM $MgCl_2$, 5mM KCl, 40% (vol/vol) glycerol, 0.25% (vol/vol) Triton X-100, 0.1mM PMSF, 0.1% (vol/vol) 2-mercaptoethanol) and 15ml 4% formaldehyde solution. 1.9ml of 2M Glycine was added to quench the formaldehyde and the mixture was incubated for another 5min under vacuum. The seedlings were snap-frozen in liquid nitrogen and ground to a fine powder. The powder from two initial tubes was pooled and suspended in 10ml NIB, with added protease inhibitor (2 tablets in 150ml NIB) (Complete Protease Inhibitor Tablets, Roche; Basel, Switzerland). The suspension was filtered twice through Miracloth (Calbiochem; EMD Milipore, Darmstadt, Germany) adding additional 10ml NIB. The filtered nuclei suspension was spun 15min at 4°C and 3000g. The supernatant was discarded and the pellet was resuspended in 4ml NIB and transferred to two 1.5ml reaction tubes. After spinning 5min, at 4°C and 1900g, the supernatant was removed and the pellet was resuspended in 1ml NIB, followed by spinning under the above conditions. This step was repeated twice. Then, the nuclei were washed twice with 1.2x NEB buffer 4 (10x NEBuffer 4: 50mM Potassium Acetate, 20mM Tris Acetate, 10mM Magnesium Acetate, 1mM Dithiothreitol (DTT)), using the centrifugation conditions described above. The nuclei were finally resuspended in 500ml 1.2x NEB buffer 4, and 5µl of 20% SDS was added. The samples were incubated for 40min at 65°C, followed by 20min at 37°C under constant shaking. 50µl of 20% Triton X-100 was added and the mixture was incubated for 1h at 37°C under constant shaking. 60µl of sample was removed as a pre-digestion control.

Digestion: 15µl 10× NEB buffer 4 and 115µlH_20 was added to the samples and digestion was started using 100 units of *Hind*III (New England Biolabs, Ipswich, USA) restriction enzyme. After three hours of incubation at 37°C, 200 units of *Hind*III were added, followed by overnight incubation at 37°C. Next morning 100 units of *Hind*III were added and samples were incubated for a final 2 h. Eighty microliters of the sample were transferred to a fresh tube and kept aside as a post-digestion control. To inactivate *Hind*III, 20 µl 20% SDS was added and samples were incubated at 65°C for 25 min under constant shaking. Samples were transferred to 15 ml conical tubes and 700 µl of 10x ligation buffer (0.5 M Tris-Cl, 0.1 M $MgCl_2$, 0.1 M DTT, pH 7.5), 375 µl of 20% Triton X-100, and H_2O to a final volume of 7 ml was added, followed by 1 h incubation at 37°C under constant shaking.

Ligation was performed by adding 70 µl of 100 mM ATP (Roche) and 50 Weiss Units of DNA Ligase (Fermentas, ThermoFisher, Waltham, USA). The sample was incubated for 5 h at 16°C. During incubation, additional 10 Weiss Units of DNA Ligase were added. Following ligation, 30 µl 10 mg/ml Proteinase K (Qbiogene, MP Biomedicals, Santa Ana, USA) were added and the samples were incubated overnight at 65°C. Next morning, 30 µl of 10 mg/ml RNase A (Roche, Basel, Switzerland) were added, and the sample was incubated for 30 min at 37°C.

The DNA was purified by two chloroform:phenol extractions, followed by ethanol precipitation using 1 ml 3 M Sodium Acetate, 7 ml H_2O, 25 µl glycogen, and ice-cold

ethanol, which was added to a final volume of 50 ml. The mixture was kept overnight at −80°C. The pellet was finally resuspended in 150 µl H_2O.

Pre-digestion control, post-digestion control, and the final 3C sample (120 ng of DNA each) were analysed on a 1.5% agarose gel. Samples with satisfactory digestion were then pooled to proceed further.

3C samples were digested with final 0.2 units/µl of the secondary restriction enzyme *Dpn*II or *Nla*II, respectively (New England Biolabs, Ipswich, USA). 4C digested samples were analysed on an agarose gel. For the 4C ligation 700 µl of T4 Ligase Buffer (Fermentas, ThermoFisher, Waltham, USA), 70 µl 100 mM ATP, 50 Weiss Units of DNA Ligase (Fermentas, ThermoFisher, Waltham, USA), and H_2O up to 7 ml was added and the ligation reaction was incubated for 5 h at 16°C. Finally, the samples were purified by phenol:chloroform extraction, followed by ethanol precipitation. 4C samples were then stored at −20°C.

For each viewpoint 16 PCRs (for detailed PCR conditions and primer sequences, see Additional file 17: Table S1) were set up, using 30 ng of 4C template for each reaction. For the ease of later Illumina library preparation, primers of a subset of samples were designed with an Illumina sequencing adapter tail (Batch 1: *MEA F6*, *MEA F8*, *PHE*, *FIS2*, *CKI1*, *FWA*, *AG, FLC*). For all other samples (Batch 2: *AT1G51860*, *AT3G44380*, *SWN*, *hk4s*, *YAO*) Illumina sequencing adapters were ligated later in the library preparation process.

An aliquot of each PCR product was analysed on an agarose gel and the remaining PCR product was purified using QIAquick PCR Purification Kit (Qiagen, Hilden, Netherlands) according to the manufacturer's protocol.

Library preparation

Hereafter library preparation is described for samples that had no Illumina (Illumina, San Diego, USA) adapter attached to the 4C primer. Samples of each replicate were pooled in equimolar amounts, and assessed on a Bioanalyzer (Agilent Technologies, Santa Clara, USA). Finally, sample volume was adjusted to 100 µl using H_20. Replicates were then split in two 50 µl aliquots. 10 µl of Resuspension buffer (RSB) (Illumina, San Diego, USA) and 40 µl End-Repair Mix (ERP) (Illumina, San Diego, USA) was added. The mixture was incubated for 30 min at 30°C. Then, 100 µl of AMPure (Agencourt, Beckman Coulter, Brea, USA) beads were added and the mixture was incubated for 15 min at RT. The reaction tubes were then placed on a magnetic stand. The supernatants were removed without disturbing the beads and 400 µl of freshly prepared 80% ethanol was added. After 30 sec ethanol was replaced with another 400 µl 80% ethanol. The supernatant was removed and the tubes were left open to dry. The beads binding the 4C PCR products were resuspended in 17.5 µl RSB and incubated for 2 min before being placed on a magnetic stand for 15 min. Finally 15 µl was transferred to a fresh 0.2 ml reaction tube. To each sample 2.5 µl of RSB and 12.5 µl A-tailing Mix (ATL) (Illumina, San Diego, USA) was added and mixed thoroughly, followed by a 30 min incubation at 37 °C. 2.5 µl of RSB, 2.5 µl of DNA Ligase Mix (LIG) (Illumina, San Diego, USA) and 2.5 µl of indexed DNA adapters (Illumina, San Diego, USA) were added and mixed gently by pipetting up and down. Subsequently, the mixture was incubated for 10 min at 30°C. To inactivate the reaction 5 µl of Stop Ligase Mix (STL) (Illumina, San Diego, USA) were added and samples were transferred to a fresh 1.5 ml reaction tube. 42.5 µl of AMPure beads (Agencourt, Beckman Coulter, Brea, USA) were added to each tube, and

the mixture was incubated for 15 min at RT. The tubes were subsequently placed on a magnetic stand for 2 min. 80 µl of supernatant were removed and replaced with 200 µl of freshly prepared 80% ethanol. After 30 sec of incubation, the supernatant was removed and the tubes were left open to dry. The previous ethanol washing step was repeated once. Then, the pellet was resuspended in 52.5 µl RSB. After 2 min of incubation at RT, tubes were placed on a magnetic stand for 2 min. 50 µl of the supernatant were transferred to a fresh 1.5 ml reaction tube. The AMPure (Agencourt, Beckman Coulter, Brea, USA) cleanup was repeated once; however, at the final step, instead of in 52.5 µl RSB the pellet was resuspended in 22.5 µl RSB, of which 20 µl were transferred to a fresh 0.2 ml reaction tube. At this point, samples with adapters already attached to the 4C PCR primers were treated in the same way. To perform final library amplification, 5 µl of PCR Primer Cocktail (PPC) (Illumina, San Diego, USA) and 25 µl of PCR Master Mix (PMM) (Illumina, San Diego, USA) were added to each tube. Then PCR was performed under the following conditions: 98°C for 30 sec; 12 cycles of 98°C for 10 sec, 60°C for 30 sec, 72°C for 30 sec, followed by a final elongation at 72°C for 5 min. Samples were then transferred to a 1.5 ml reaction tube and 50 ml of AMPure (Agencourt, Beckman Coulter, Brea, USA) beads were added. After 15 min of incubation at RT, the tubes were placed on a magnetic stand for 2 min. Ninety-five microliters of supernatant were removed and the beads were washed twice with 200 µl of freshly prepared 80% ethanol. After removing the supernatant, tubes were left open to dry. The pellet was then resuspended in 32.5 µl RSB and incubated for 2 min at RT. The tubes were placed on a magnetic stand and 30 µl of the purified library were transferred to a fresh 1.5 ml reaction tube. Of each library a 10 nM stock in Tris-Cl (pH8.5) with 0.1 Tween 20 was prepared. The libraries were subsequently pooled by replicates and passed on to Illumina HiSeq 100 bp single end sequencing. For each batch of replicates, one lane per replicate was loaded (total of four lanes). Batch 1 replicate A had a total yield of 92’063’669 raw reads with a mean quality score of 35.35. Batch 1 replicate B had a total yield of 80’777’012 raw reads with a mean quality score of 35.31. Batch 2 replicate A had a total yield of 43’296’252 raw reads with a mean quality score of 36.85. Batch 2 replicate B had a total yield of 55’187’969 raw reads with a mean quality score of 36.76.

4C sequencing data pre-processing

The two fastq files (one per replicate) were split into separate viewpoints according to the 4C primer sequences and the *Hind*III restriction pattern within the reads. No mismatches were allowed and the remaining reads were discarded. After removal of primer and restriction site sequences, reads were trimmed to 30 bp and aligned to the *Arabidopsis* reference genome [48] using bowtie (version 0.12.7) [49] with the command line arguments -a -v 0 -m 25. Alignment statistics are given in Additional file 17: Table S2.

Reads with multiple alignments were processed as described previously [50]. Since we estimated the length of a single interaction unit as 100 kb, we used an allocation distance of ± 50 kb. To specify potential 4C fragments, we generated an *in silico Hind*III digest of the *Arabidopsis* Col-0 genome. Reads mapping to the ends of the resulting fragments were considered for further analysis. For a more robust measure of interactions, fragments were then used to generate windows spanning a larger region of the genome (i.e. 100 fragments corresponding to 180 kb on average). During this process, fragments closer than 1 kb to the viewpoint were discarded given that a large proportion of their reads likely originates from incomplete digestion and/or self-circularization. Furthermore, we discarded all fragments closer than 100 kb to a centromere as the quality of alignments to centromeres is low. Finally, fragments whose distance from the primary restriction site to the first occurring secondary

restriction site was ≥ 1000 bp with respect to both ends of the fragment were removed as well. As a measure of interaction of a given window ("interaction value"), fragment counts were log-transformed to avoid high impact of outlier fragments and then summed up. Depending on the downstream analysis, windows were spanning either 100 fragments from each fragment on (overlapping) or 25 fragments from every 25th fragment.

Processed 4C data files (split according to primer sequence) and raw-data sequencing files are publically available on Gene Expression Omnibus (GEO) accession number GSE50181.

Histone modifications, transcription, DNA methylation, and genomic sequencing data processing

To add additional information, such as histone modification patterns and transcription rates, we obtained publicly available data from GEO [51], specifically ChIP-seq data GSM701923, GSM701924, GSM701925, GSM701926, GSM701927, GSM701928, GSM701929, GSM701930, GSM701931 [30], and RNA-seq data GSM701934 [30]. Pre-processed DNA methylation data was obtained from [32].

ChIP-seq and RNA-seq reads (SOLiD, 50 bp) were aligned to the *Arabidopsis* reference genome (Col-0, TAIR10) using bowtie (version 0.12.7) with following options: –a –v 2 –m 25. Reads with multiple alignments were processed as described previously [50]. Allocation distances were set to ± 5 kb and ± 50 bp for the ChIP-seq and the RNA-seq data, respectively. Histone modification densities and DNA methylation densities were calculated by the sum of nucleotides covered with at least one uniquely alignable short sequence, divided by the total number of nucleotides for each individual 4C restriction fragment.

To estimate potential biases related to sequence composition (e.g. repetitive sequences), we obtained genomic DNA sequencing data (Illumina, 100 bp) GSM567816 and processed them identically as the 4C sequencing data.

Assigning *P*-values to individual windows

To estimate the significance of an interaction, we calculated for each window the probability (i.e. *P*-values) to observe its interaction value by chance. Given that an interaction of two fragments would lead to a higher read count in the neighbouring fragments as well (hence in the window), random shuffling of fragment positions and recalculation of window interaction values provides randomised interaction data with the values following a normal distribution. Using the parameters of this distribution, a preliminary *P*-value was then calculated for each window. We repeated this process 1000 times and averaged for each window the *P*-values from all individual repetitions to obtain a final *P*-value. To take into account the differences between chromosome arms (e.g. the different amount of DNA between the short arm and the long arm of chromosome 2), the *P*-values were calculated for each chromosome arm separately.

Threshold of *P*-values were chosen to best fulfil either requirements of plotting or data analysis. Generally, we set the threshold for prey regions to 10^{-3}. In the Circos plot of Figure 5A we chose $P \leq 10^{-4}$ for better visibility. As for various viewpoints a threshold of 10^{-3} did not yield a sufficient number of prey regions for robust data analysis, we chose a threshold of $P \leq 0.05$ to perform PCA.

Distance decay

We estimated the genomic distance-dependent decay of interaction probability on a distance of 1 kb – 10 Mb from the viewpoint. This stretch was log-transformed and split into 41 intervals with length 0.1 (on the log scale). For each sample, the reads of the fragments corresponding to the intervals were summed up and assigned to the interval. Given that the centromere acts as an interaction boundary, only fragments on the viewpoint's arm were considered. Read counts per interval were then divided by the total number of reads across all intervals representing contact probabilities, which across the full distance add up to 1. Given that some intervals only contained few fragments and, in certain cases, only fragments from a subset of the viewpoints, we used a LOESS predictor fitted to the original data to calculate one single contact probability value for each interval. To obtain the slope, and hence the distance decay coefficient, we then approximated the data with a linear model. Slope and *P*-value were derived from the fit of the linear model to the values predicted with the LOESS fit. However, direct fitting of a linear model to the original data yielded almost equal results with a slope of −0.72 instead of −0.73 and an extremely low *P*-value ($< 10^{-100}$).

Centromere distance

To analyse the effect of a viewpoint's distance to the centromere on the distribution of the observed interaction frequencies along chromosome arms, we calculated for each chromosome arm (except the viewpoint's arm) the distance to the centromere at which 50% of all reads are aligned, and then fitted a linear model. The procedure was performed twice, first using absolute values, and then relative distances defined as the absolute distance divided by the length of the chromosome arm (transformed by taking the arcsine of the square root).

Principal component analyses (PCA)

All PCA-related analyses were based on non-overlapping windows including 25 fragments. For each viewpoint, mean prey and control histone densities for each histone modification (epigenetic modification density, EMD) were calculated. Subsequently, PCA was performed on a data set including mean EMD values of control and prey regions for each viewpoint and EMD. PCA was performed using build-in R princomp() function.

Permutation test

To analyze differences in the epigenetic landscape of prey and control regions, we randomly selected 50 prey and 50 control regions (sampled) for each viewpoint and obtained a corresponding randomized test set by pooling their EMDs and permuting them (shuffling them into two randomized groups of 50 values each). We then calculated the absolute differences in averaged EMDs between the sampled ($RealDiff_{ij}$), and the permutated ($RandDiff_{ij}$) prey and control regions, respectively.

Repeating this step *i* times for each of the *j* viewpoints yielded an empirical distribution for RandDiff for every epigenetic modification with 13'000 values (j = 13 viewpoints, and i = 1'000 repetitions). Comparing the average $RealDiff_m$ (mean across all repetitions and viewpoints) to this distribution then provided an empirical *P*-value ($p = \sum(RandDiff_{ij} >$

$RealDiff_m$)/(i*j)), which were subsequently adjusted for multiple testing calculating false discovery rate (FDR – Benjamini-Hochberg).

Analysis of individual epigenetic marks employing GSEA-like analysis

To test whether prey regions have a different epigenetic landscape compared to regions chosen randomly across the genome, we developed a procedure similar to the Gene Set Enrichment Analysis (GSEA) described in [33]. It requires densities of epigenetic modifications (EMDs, e.g. CG methylation density or H3K9me2) assigned to all (n) regions in the genome (i.e. non-overlapping windows spanning 25 restriction fragments), and a subset of the (m) regions as a test set (i.e. prey regions with a P-value < 0.01 in both replicates). During the procedure, the regions are first sorted according to their EMD. We then assign a value of −1 to regions not in the test set, and a value of $(n\text{-}m)/m$ to the regions in the test set (to assure that the sum of these values across all regions is zero). In a third step, the cummulative sum of these values is calculated and the enrichment score (ES) is defined as the maximum (absolute) deviation from zero. If the regions in the test set were randomly distributed across the sorted list of all regions, the cumulative sum would fluctuate around zero with a relatively small ES. Conversely, a non-random distribution of the test set (e.g. accumulation at one end of the sorted list) would lead to a high ES. A P-value can then be assigned by comparing an observed ES to an ES distribution obtained by randomly choosing m regions for 10'000 times. To obtain one P-value per epigenetic feature, the ES were averaged across all viewpoints. As we were focusing on long-range interactions, we excluded all interactions within the viewpoint's arm. As statistical testing for all epigenetic features was employed using the same 4C data, P-values were adjusted for multiple testing calculating FDR (Benjamini-Hochberg).

Plotting

All plotting of 4C data, genomic features and histone modification data was performed using either Circos [23] or built-in R functions [52] plotting. Code is available upon request.

Data availability

All sequencing data and processed 4C files are available on Gene Expression Omnibus (GEO) accession number GSE50181.

Abbreviations

4C: Circular chromosome conformation capture; EMD: Epigenetic modification density; RT: Room temperature; sd: Standard deviation

Competing interests

The authors declare that they have no competing interests.

Authors' contributions

SG conceived the study, conducted the experiments, performed data analysis, and wrote the manuscript. MWS performed data analysis and helped to write the manuscript. TW helped to conceive the study and helped to edit the manuscript, NL helped to conceive the study. UG conceived the study and helped with data interpretation and writing of the manuscript. All authors read and approved the final manuscript.

Acknowledgements

We thank Keith Harshman, Johann Weber and Corinne Peter (University of Lausanne) for advice on Illumina library construction, and Heike Lindner, Aurélien Boisson-Dernier and Pauline Jullien for critically reading the manuscript. This work was supported by the University of Zürich, the University Research Priority Program Functional Genomics/Systems Biology, an IPhD project grant from SystemsX.ch, the Swiss Initiative for Systems Biology (to U.G., T.W., N.L.), and an Advanced Grant of the European Research Council (to U.G.).

References

1. Dittmer TA, Stacey NJ, Sugimoto-Shirasu K, Richards EJ: ***LITTLE NUCLEI* genes affecting nuclear morphology in *Arabidopsis thaliana*.** *Plant Cell* 2007, **19:**2793–2803.

2. Arnott S, Hukins DW: **Optimised parameters for A-DNA and B-DNA.** *Biochem Biophys Res Commun* 1972, **47:**1504–1509.

3. Roudier FCO, Ahmed I, Rard CBE, Sarazin A, Mary-Huard T, Cortijo S, Bouyer D, Caillieux E, Duvernois-Berthet E, Al-Shikhley L, Giraut LEN, s BDE, Drevensek SEP, Barneche FED, Rozier SDE, Brunaud VER, Aubourg SEB, Schnittger A, Bowler C, Martin-Magniette M-L, Robin SEP, Caboche M, Colot V: **Integrative epigenomic mapping defines four main chromatin states in *Arabidopsis*.** *EMBO J* 2011, **30:**1928–1938.

4. Filion GJ, van Bemmel JG, Braunschweig U, Talhout W, Kind J, Ward LD, Brugman W, de Castro IJ, Kerkhoven RM, Bussemaker HJ, van Steensel B: **Systematic protein location mapping reveals five principal chromatin types in *Drosophila* cells.** *Cell* 2010, **143:**212–224.

5. Pfluger J, Wagner D: **Histone modifications and dynamic regulation of genome accessibility in plants.** *Curr Opin Plant Biol* 2007, **10:**645–652.

6. Rabl C: **Über die Zelltheilung.** *Morphologisches Jahrbuch* 1885, **10:**214–330.

7. Heitz E: **Das Heterochromatin der Moose.** *1 Jahrb Wiss Bot* 1929, **69:**762–818.

8. La Cour L: **Heterochromatin and the organization of nucleoli in plants.** *Heredity* 1951, **5:**37.

9. Noordermeer D, Leleu M, Splinter E, Rougemont J, De Laat W, Duboule D: **The dynamic architecture of *Hox* gene clusters.** *Science* 2011, **334:**222–225.

10. Gheldof N, Smith EM, Tabuchi TM, Koch CM, Dunham I, Stamatoyannopoulos JA, Dekker J: **Cell-type-specific long-range looping interactions identify distant regulatory elements of the CFTR gene.** *Nucleic Acids Res* 2010, **38:**4325–4336.

11. McClintock B: **Chromosome morphology in *Zea mays*.** *Science* 1929, **69:**629.

12. Fransz PF, Armstrong S, de Jong JH, Parnell LD, van Drunen C, Dean C, Zabel P, Bisseling T, Jones GH: **Integrated cytogenetic map of chromosome arm 4S of *A. thaliana*: structural organization of heterochromatic knob and centromere region.** *Cell* 2000, **100:**367–376.

13. Laboratory TCSH, Washington University Genome Sequencing Center, Consortium PBAS: **The complete sequence of a heterochromatic island from a higher eukaryote.** *Cell* 2000, **100:**377–386.

14. Fransz P, Armstrong S, Alonso-Blanco C, Fischer TC, Torres-Ruiz RA, Jones G: **Cytogenetics for the model system *Arabidopsis thaliana*.** *Plant J* 1998, **13:**867–876.

15. Dekker J, Rippe K, Dekker M, Kleckner N: **Capturing chromosome conformation.** *Science* 2002, **295:**1306–1311.

16. De Wit E, De Laat W: **A decade of 3C technologies: insights into nuclear organization.** *Genes Dev* 2012, **26:**11–24.

17. Zhao Z, Tavoosidana G, Sjölinder M, Göndör A, Mariano P, Wang S, Kanduri C, Lezcano M, Sandhu KS, Singh U, Pant V, Tiwari V, Kurukuti S, Ohlsson R: **Circular chromosome conformation capture (4C) uncovers extensive networks of epigenetically regulated intra- and interchromosomal interactions.** *Nat Genet* 2006, **38:**1341–1347.

18. Lieberman-Aiden E, Van Berkum NL, Williams L, Imakaev M, Ragoczy T, Telling A, Amit I, Lajoie BR, Sabo PJ, Dorschner MO, Sandstrom R, Bernstein B, Bender MA, Groudine M, Gnirke A, Stamatoyannopoulos J, Mirny LA, Lander ES, Dekker J: **Comprehensive mapping of long-range interactions reveals folding principles of the human genome.** *Science* 2009, **326:**289–293.

19. Louwers M, Bader R, Haring M, Van Driel R, De Laat W, Stam M: **Tissue- and expression level-specific chromatin looping at maize *b1* epialleles.** *Plant Cell* 2009, **21:**832–842.

20. Moissiard G, Cokus SJ, Cary J, Feng S, Billi AC, Stroud H, Husmann D, Zhan Y, Lajoie BR, McCord RP, Hale CJ, Feng W, Michaels SD, Frand AR, Pellegrini M, Dekker J, Kim JK, Jacobsen S: **MORC family ATPases required for heterochromatin condensation and gene silencing.** *Science* 2012, **336:**1448–1451.

21. Crevillen P, Sonmez C, Wu Z, Dean C: **A gene loop containing the floral repressor *FLC* is disrupted in the early phase of vernalization.** *EMBO J* 2012, **32:**140–148.

22. Sexton T, Yaffe E, Kenigsberg E, Bantignies F, Leblanc B, Hoichman M, Parrinello H, Tanay A, Cavalli G: **Three-dimensional folding and functional organization principles of the *Drosophila* genome.** *Cell* 2012, **148:**458–472.

23. Krzywinski M, Schein J, Birol I, Connors J, Gascoyne R, Horsman D, Jones SJ, Marra MA: **Circos: An information aesthetic for comparative genomics.** *Genome Res* 2009, **19:**1639–1645.

24. Splinter E, de Wit E, van de Werken HJG, Klous P, De Laat W: **Determining long-range chromatin interactions for selected genomic sites using 4C-seq technology: From fixation to computation.** *Methods* 2012, **58:**221–230.

25. Hou H, Zhou Z, Wang Y, Wang J, Kallgren SP, Kurchuk T, Miller EA, Chang F, Jia S: **Csi1 links centromeres to the nuclear envelope for centromere clustering.** *J Cell Biol* 2012, **199:**735–744.

26. de Nooijer S, Wellink J, Mulder B, Bisseling T: **Non-specific interactions are sufficient to explain the position of heterochromatic chromocenters and nucleoli in interphase nuclei.** *Nucleic Acids Res* 2009, **37:**3558–3568.

27. Fransz P, De Jong JH, Lysak M, Castiglione MR, Schubert I: **Interphase chromosomes in *Arabidopsis* are organized as well defined chromocenters from which euchromatin loops emanate.** *Proc Natl Acad Sci U S A* 2002, **99:**14584–14589.

28. Fang Y, Spector DL: **Centromere positioning and dynamics in living *Arabidopsis* plants.** *Mol Biol Cell* 2005, **16:**5710–5718.

29. Gheldof N, Tabuchi TM, Dekker J: **The active *FMR1* promoter is associated with a large domain of altered chromatin conformation with embedded local histone modifications.** *Proc Natl Acad Sci U S A* 2006, **103:**12463–12468.

30. Tolhuis B, Blom M, Kerkhoven RM, Pagie L, Teunissen H, Nieuwland M, Simonis M, De Laat W, van Lohuizen M, van Steensel B: **Interactions among *Polycomb* domains are guided by chromosome architecture.** *PLoS Genet* 2011, **7:**e1001343.

31. Luo C, Sidote DJ, Zhang Y, Kerstetter RA, Michael TP, Lam E: **Integrative analysis of chromatin states in *Arabidopsis* identified potential regulatory mechanisms for natural antisense transcript production.** *Plant J* 2012, **73:**77–90.

32. Stroud H, Greenberg MVC, Feng S, Bernatavichute YV, Jacobsen SE: **Comprehensive analysis of silencing mutants reveals complex regulation of the *Arabidopsis* methylome.** *Cell* 2013, **152:**352–364.

33. Subramanian A, Tamayo P, Mootha VK, Mukherjee S, Ebert BL, Gillette MA, Paulovich A, Pomeroy SL, Golub TR, Lander ES, Mesirov JP: **Gene set enrichment analysis: a knowledge-based approach for interpreting genome-wide expression profiles.** *Proc Natl Acad Sci U S A* 2005, **102:**15545–15550.

34. La Bastide De M, Huang E, Spiegel L, Gnoj L, Tabata S, Kaneko T, Nakamura Y, Kotani H, Kato T, Asamizu E, Miyajima N, Sasamoto S, Kimura T, Hosouchi T, Kawashima K,

Kohara M, Matsumoto M, Matsuno A, Muraki A, Nakayama S, Nakazaki N, Naruo K, Okumura S, Shinpo S, Takeuchi C, Wada T, Watanabe A, Yamada M, Yasuda M, Sato S, *et al*: **Sequence and analysis of chromosome 5 of the plant *Arabidopsis thaliana*.** *Nature* 2000, **408:**823–826.

35. Maul GG, Deaven L: **Quantitative determination of nuclear pore complexes in cycling cells with differing DNA content.** *J Cell Biol* 1977, **73:**748–760.

36. Schubert V, Berr A, Meister A: **Interphase chromatin organisation in *Arabidopsis* nuclei: constraints versus randomness.** *Chromosoma* 2012, **121:**369–387.

37. Jin QW, Fuchs J, Loidl J: **Centromere clustering is a major determinant of yeast interphase nuclear organization.** *J Cell Sci* 2000, **113:**1903–1912.

38. Duan Z, Andronescu M, Schutz K, Mcilwain S, Kim YJ, Lee C, Shendure J, Fields S, Blau CA, Noble WS: **A three-dimensional model of the yeast genome.** *Nature* 2010, **465:**363–367.

39. Sanyal A, Baù D, Marti-Renom MA, Dekker J: **Chromatin globules: a common motif of higher order chromosome structure?** *Curr Opin Cell Biol* 2011, **23:**325–331.

40. Armstrong SJ, Franklin FC, Jones GH: **Nucleolus-associated telomere clustering and pairing precede meiotic chromosome synapsis in *Arabidopsis thaliana*.** *J Cell Sci* 2001, **114:**4207–4217.

41. Watanabe K, Pecinka A, Meister A, Schubert I, Lam E: **DNA hypomethylation reduces homologous pairing of inserted tandem repeat arrays in somatic nuclei of *Arabidopsis thaliana*.** *Plant J* 2005, **44:**531–540.

42. Wolfgruber TK, Sharma A, Schneider KL, Albert PS, Koo D-H, Shi J, Gao Z, Han F, Lee H, Xu R, Allison J, Birchler JA, Jiang J, Dawe RK, Presting GG: **Maize centromere structure and evolution: Sequence analysis of centromeres 2 and 5 reveals dynamic loci shaped primarily by retrotransposons.** *PLoS Genet* 2009, **5:**e1000743.

43. Nagaki K, Song J, Stupar RM, Parokonny AS, Yuan Q, Ouyang S, Liu J, Hsiao J, Jones KM, Dawe RK, Buell CR, Jiang J: **Molecular and cytological analyses of large tracks of centromeric DNA reveal the structure and evolutionary dynamics of maize centromeres.** *Genetics* 2003, **163:**759–770.

44. Henikoff S: **The centromere paradox: Stable inheritance with rapidly evolving DNA.** *Science* 2001, **293:**1098–1102.

45. Berr A, Pecinka A, Meister A, Kreth G, Fuchs J, Blattner FR, Lysak MA, Schubert I: **Chromosome arrangement and nuclear architecture but not centromeric sequences are conserved between *Arabidopsis thaliana* and *Arabidopsis lyrata*.** *Plant J* 2006, **48:**771–783.

46. Nagaki K, Talbert PB, Zhong CX, Dawe RK, Henikoff S, Jiang J: **Chromatin immunoprecipitation reveals that the 180-bp satellite repeat is the key functional DNA element of *Arabidopsis thaliana* centromeres.** *Genetics* 2003, **163:**1221–1225.

47. Shibata F: **Differential localization of the centromere-specific proteins in the major centromeric satellite of *Arabidopsis thaliana*.** *J Cell Sci* 2004, **117:**2963–2970.

48. Huala E, Dickerman AW, Garcia-Hernandez M, Weems D, Reiser L, LaFond F, Hanley D, Kiphart D, Zhuang M, Huang W, Mueller LA, Bhattacharyya D, Bhaya D, Sobral BW, Beavis W, Meinke DW, Town CD, Somerville C, Rhee SY: **The Arabidopsis Information Resource (TAIR): a comprehensive database and web-based information retrieval, analysis, and visualization system for a model plant.** *Nucleic Acids Res* 2001, **29:**102–105.

49. Langmead B, Trapnell C, Pop M, Salzberg SL: **Ultrafast and memory-efficient alignment of short DNA sequences to the human genome.** *Genome Biol* 2009, **10:**R25.

50. Schmid MW, Schmidt A, Klostermeier UC, Barann M, Rosenstiel P, Grossniklaus U: **A powerful method for transcriptional profiling of specific cell types in eukaryotes: Laser-assisted microdissection and RNA sequencing.** *PLoS ONE* 2012, **7:**e29685.

51. Edgar R, Domrachev M, Lash AE: **Gene Expression Omnibus: NCBI gene expression and hybridization array data repository.** *Nucleic Acids Res* 2002, **30:**207–10.

52. R Development Core Team: *R: A language and environment for statistical computing.* Vienna, Austria: R Foundation for Statistical Computing; 2008. http://www.R-project.org. ISBN 3-900051-07-0.

Additional files

Additional_file_1 as PDF
Additional file 1: Figure S1 4C interactome of MEA F6.

Additional_file_2 as PDF
Additional file 2: Figure S2 4C interactome of MEA F8.

Additional_file_3 as PDF
Additional file 3: Figure S3 4C interactome of AT1G51860.

Additional_file_4 as PDF
Additional file 4: Figure S4 4C interactome of PHE1.

Additional_file_5 as PDF
Additional file 5: Figure S5 4C interactome of FIS2.

Additional_file_6 as PDF
Additional file 6: Figure S6 4C interactome of *CKI1*.

Additional_file_7 as PDF
Additional file 7: Figure S7 4C interactome of *AT3G44380*.

Additional_file_8 as PDF
Additional file 8: Figure S8 4C interactome of *SWN*.

Additional_file_9 as PDF
Additional file 9:Figure S9 4C interactome of hk4s.

Additional_file_10 as PDF
Additional file 10: Figure S10 4C interactome of YAO.

Additional_file_11 as PDF
Additional file 11: Figure S11 4C interactome of AG.

Additional_file_12 as PDF
Additional file 12: Figure S12 4C interactome of FWA.

Additional_file_13 as PDF
Additional file 13: Figure S13 4C interactome of FLC.

Additional_file_14 as PDF
Additional file 14: Figure S15 PCA for individual viewpoints. Each graph represents a biplot of a PCA including histone modification densities for prey and control regions of a given viewpoint, respectively. Contribution to the variance of the first two principal components are indicated below the biplot. Loadings of the four major factors to the first principal component are listed.

Additional_file_15 as PDF
Additional file 15: Figure S16 Epigenetic modification densities (EMD). For each EMD and viewpoint, the mean EMD for 1000 times randomly chosen 50 prey and control regions was calculated and plotted. Green bars: prey, yellow bars: control.

Additional_file_16 as PDF
Additional file 16: Figure S14 Interaction frequency decay for individual viewpoints. Interaction frequency decay is plotted for individual viewpoints. Black line: LOESS smoothened decay. Red dotted line: Linear regression. Values of the slopes are indicated in the lower left corner of each graph.

Additional_file_17 as DOCX
Additional file 17 Table S1 Viewpoint coordinates and primer sequences. Indicated are the viewpoints' names, their respective chromosome and position in bp, primer sequences and restriction enzymes used for primary (1°RS) and secondary (2°RS) digest, respectively. **Table S2**, Alignment scores. Columns indicating chromosomes show numbers of mapped reads. Other columns: unmapped reads, percentage of mapped reads, and total of reads.

Figure 1

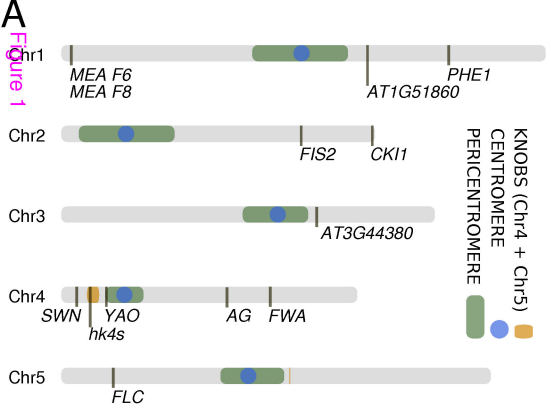
A
Chr1
MEA F6
MEA F8
AT1G51860
PHE1
Chr2
FIS2
CKI1
Chr3
AT3G44380
Chr4
SWN
YAO
hk4s
AG
FWA
Chr5
FLC
KNOBS (Chr4 + Chr5)
CENTROMERE
PERICENTROMERE

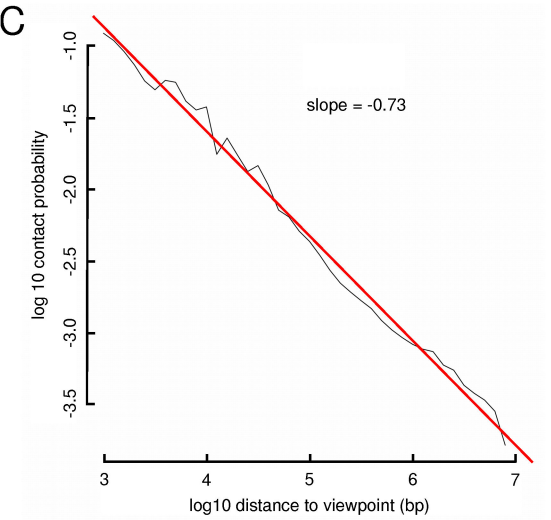
C
slope = -0.73
log 10 contact probability
-1.0
-1.5
-2.0
-2.5
-3.0
-3.5
3
4
5
6
7
log10 distance to viewpoint (bp)

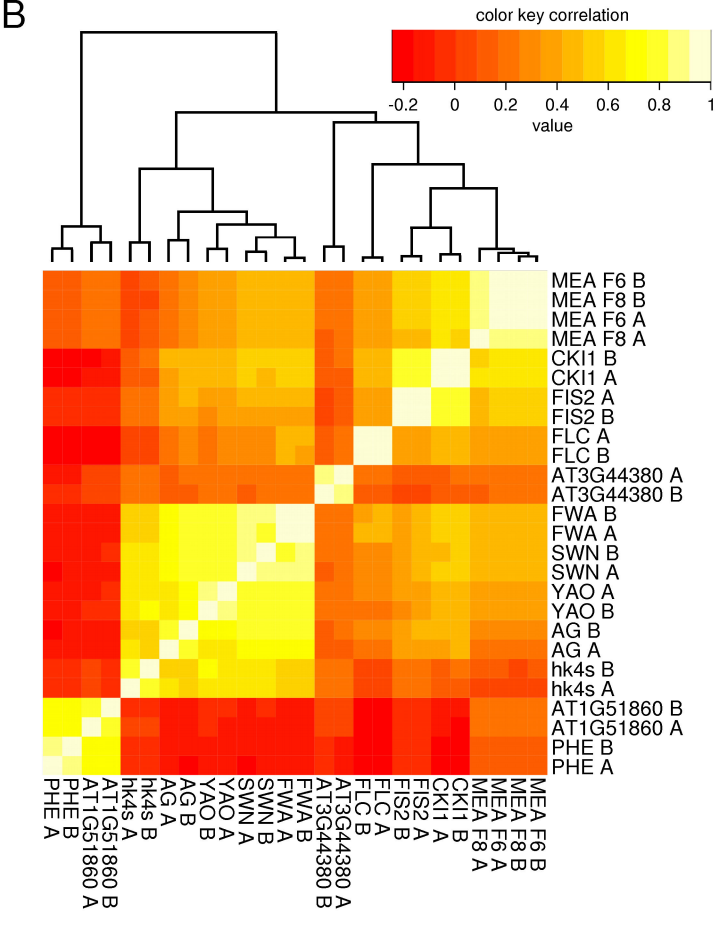
B
color key correlation
-0.2
0
0.2
0.4
0.6
0.8
1
value
MEA F6 B
MEA F8 B
MEA F6 A
MEA F8 A
CKI1 B
CKI1 A
FIS2 A
FIS2 B
FLC A
FLC B
AT3G44380 A
AT3G44380 B
FWA B
FWA A
SWN B
SWN A
YAO A
YAO B
AG B
AG A
hk4s B
hk4s A
AT1G51860 B
AT1G51860 A
PHE B
PHE A

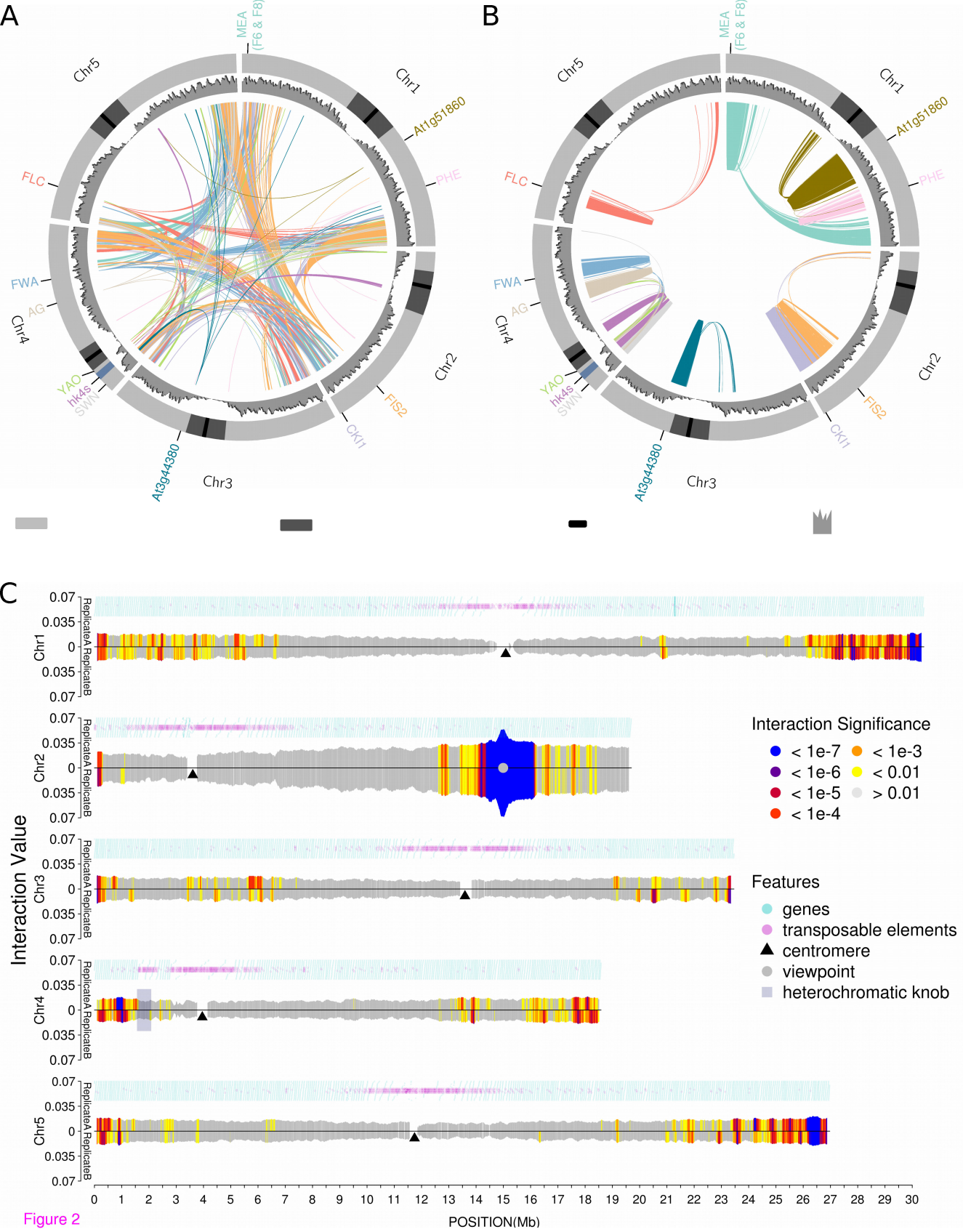
A
B
C
MEA
(F6 & F8)
Chr1
At1g51860
PHE
Chr2
FIS2
CK1
At3g44380
Chr3
FLC
Chr5
FWA
AG
Chr4
YAO
hk4s
SWN
Interaction Value
ReplicateA
ReplicateB
Interaction Significance
< 1e-7
< 1e-6
< 1e-5
< 1e-4
< 1e-3
< 0.01
> 0.01
Features
genes
transposable elements
centromere
viewpoint
heterochromatic knob
POSITION(Mb)

Figure 2

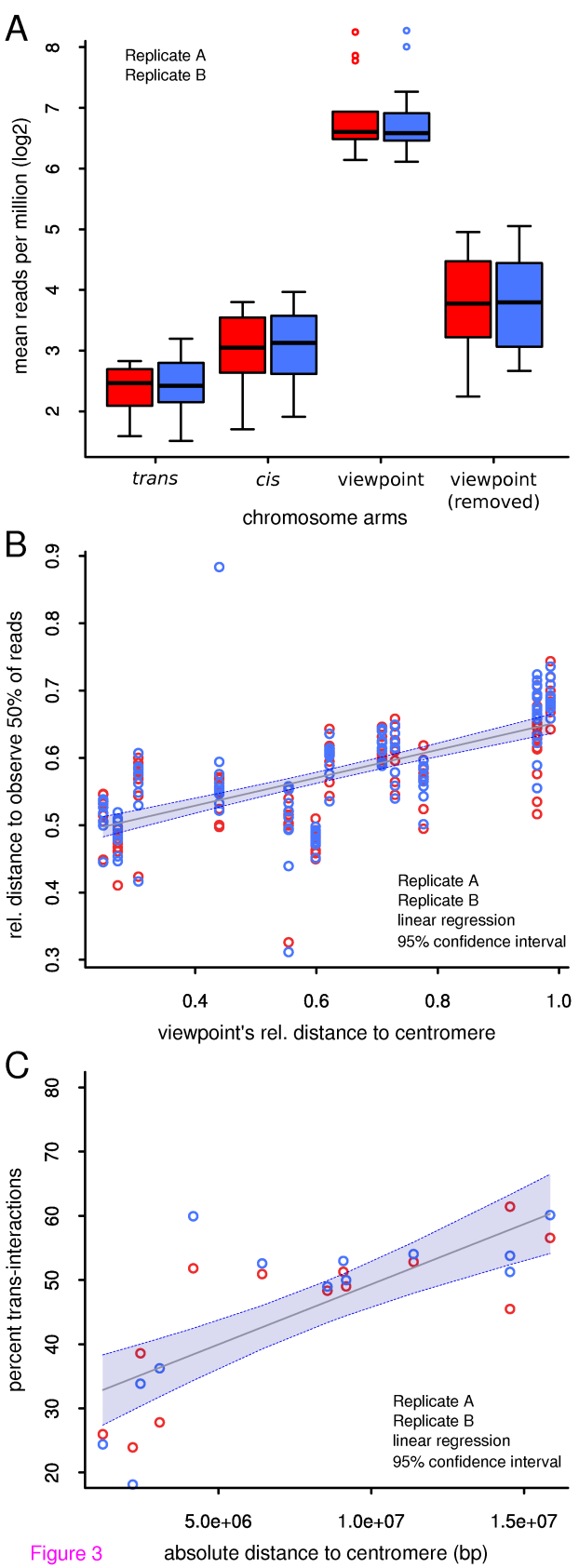
A
Replicate A
Replicate B
mean reads per million (log2)
2
3
4
5
6
7
8
trans
cis
viewpoint
viewpoint (removed)
chromosome arms
B
rel. distance to observe 50% of reads
0.3
0.4
0.5
0.6
0.7
0.8
0.9
Replicate A
Replicate B
linear regression
95% confidence interval
0.4
0.6
0.8
1.0
viewpoint's rel. distance to centromere
C
percent trans-interactions
20
30
40
50
60
70
80
Replicate A
Replicate B
linear regression
95% confidence interval
5.0e+06
1.0e+07
1.5e+07
absolute distance to centromere (bp)

Figure 3

Figure 4

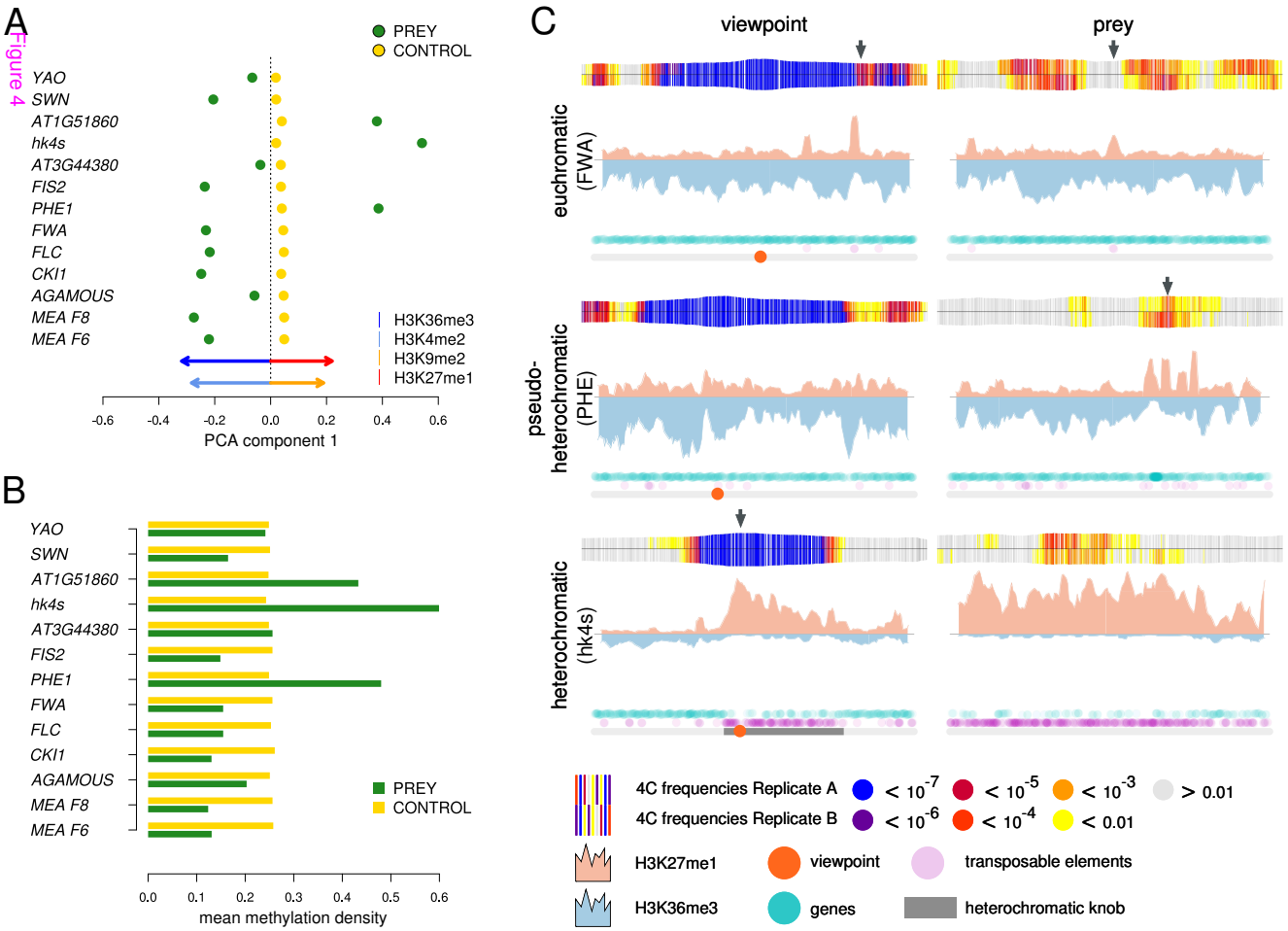
A
PREY
CONTROL
YAO
SWN
AT1G51860
hk4s
AT3G44380
FIS2
PHE1
FWA
FLC
CKI1
AGAMOUS
MEA F8
MEA F6
H3K36me3
H3K4me2
H3K9me2
H3K27me1
-0.6 -0.4 -0.2 0.0 0.2 0.4 0.6
PCA component 1
B
YAO
SWN
AT1G51860
hk4s
AT3G44380
FIS2
PHE1
FWA
FLC
CKI1
AGAMOUS
MEA F8
MEA F6
PREY
CONTROL
0.0 0.1 0.2 0.3 0.4 0.5 0.6
mean methylation density
C
viewpoint
prey
euchromatic (FWA)
pseudo-heterochromatic (PHE)
heterochromatic (hk4s)
4C frequencies Replicate A
4C frequencies Replicate B
< 10-7
< 10-6
< 10-5
< 10-4
< 10-3
< 0.01
> 0.01
H3K27me1
H3K36me3
viewpoint
genes
transposable elements
heterochromatic knob

Figure 5

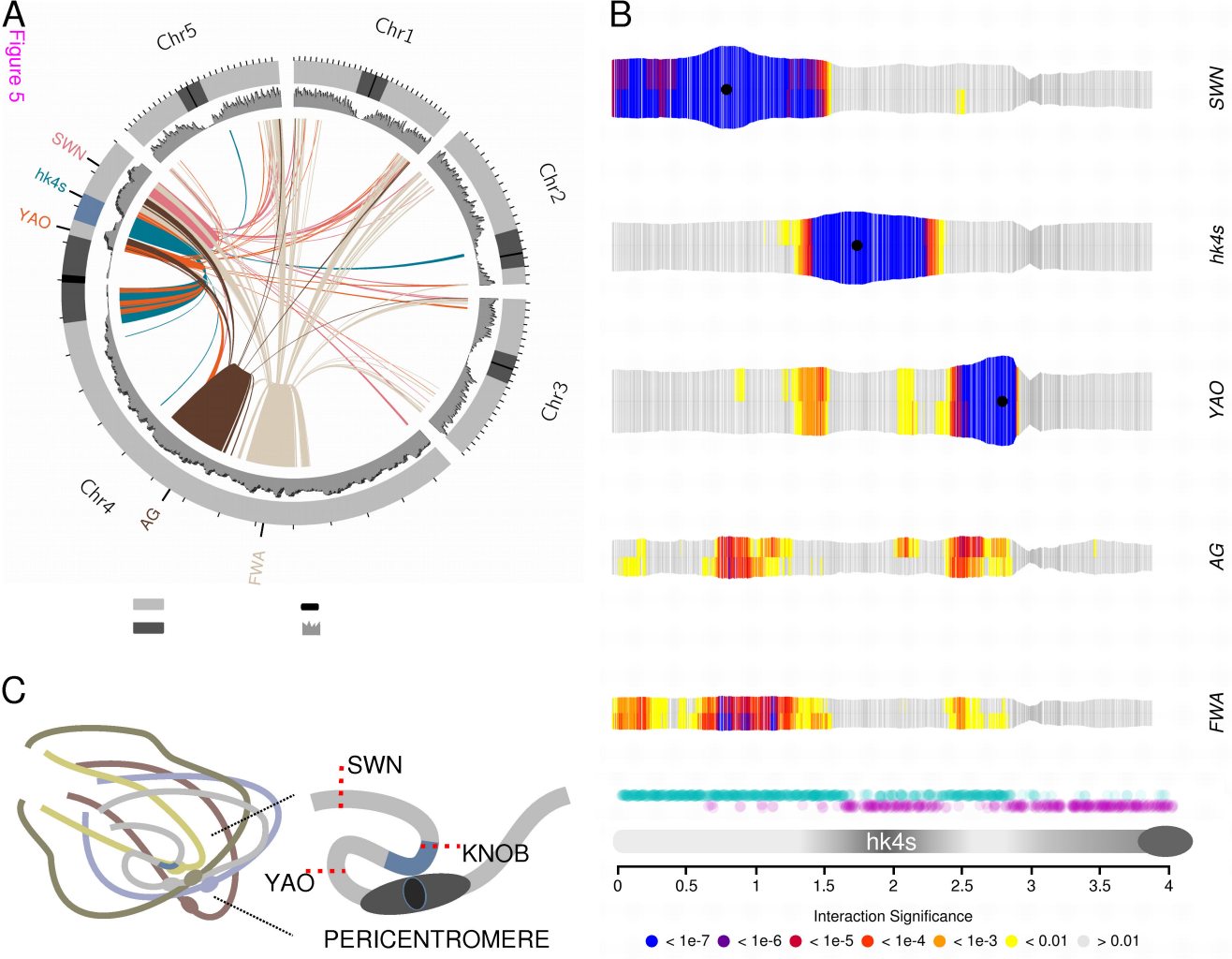
A
Chr5
Chr1
Chr2
Chr3
Chr4
SWN
hk4s
YAO
AG
FWA
B
SWN
hk4s
YAO
AG
FWA
hk4s
0
0.5
1
1.5
2
2.5
3
3.5
4
Interaction Significance
< 1e-7
< 1e-6
< 1e-5
< 1e-4
< 1e-3
< 0.01
> 0.01
C
SWN
KNOB
YAO
PERICENTROMERE

Additional files provided with this submission:

Additional file 1: 1842658369102075_add1.pdf, 4277K
http://genomebiology.com/imedia/8547750131139770/supp1.pdf
Additional file 2: 1842658369102075_add2.pdf, 4480K
http://genomebiology.com/imedia/5478693721139771/supp2.pdf
Additional file 3: 1842658369102075_add3.pdf, 4229K
http://genomebiology.com/imedia/3162487311139771/supp3.pdf
Additional file 4: 1842658369102075_add4.pdf, 4184K
http://genomebiology.com/imedia/1966405583113977/supp4.pdf
Additional file 5: 1842658369102075_add5.pdf, 4125K
http://genomebiology.com/imedia/1323894570113977/supp5.pdf
Additional file 6: 1842658369102075_add6.pdf, 4259K
http://genomebiology.com/imedia/4945102521139771/supp6.pdf
Additional file 7: 1842658369102075_add7.pdf, 4332K
http://genomebiology.com/imedia/9478830861139771/supp7.pdf
Additional file 8: 1842658369102075_add8.pdf, 4165K
http://genomebiology.com/imedia/8181131981139771/supp8.pdf
Additional file 9: 1842658369102075_add9.pdf, 3958K
http://genomebiology.com/imedia/9972909161139771/supp9.pdf
Additional file 10: 1842658369102075_add10.pdf, 4187K
http://genomebiology.com/imedia/1853120334113977/supp10.pdf
Additional file 11: 1842658369102075_add11.pdf, 4393K
http://genomebiology.com/imedia/1450480921113977/supp11.pdf
Additional file 12: 1842658369102075_add12.pdf, 3962K
http://genomebiology.com/imedia/1722111433113977/supp12.pdf
Additional file 13: 1842658369102075_add13.pdf, 4121K
http://genomebiology.com/imedia/1030461903113977/supp13.pdf
Additional file 14: 1842658369102075_add14.pdf, 709K
http://genomebiology.com/imedia/5321317211139771/supp14.pdf
Additional file 15: 1842658369102075_add15.pdf, 154K
http://genomebiology.com/imedia/1207354723113977/supp15.pdf
Additional file 16: 1842658369102075_add16.pdf, 312K
http://genomebiology.com/imedia/1927324413113977/supp16.pdf
Additional file 17: 1842658369102075_add17.docx, 18K
http://genomebiology.com/imedia/9383354781139771/supp17.docx